International Journal of Earth Sciences (2021) 110:81–111
https://doi.org/10.1007/s00531-020-01939-0

ORIGINAL PAPER

Early Paleozoic structural and metamorphic evolution of the Transpatagonian Orogen related to Gondwana assembly

Pablo D. González[1] · Maximiliano Naipauer[2] · Ana M. Sato[3] · Ricardo Varela[3] · Miguel A. S. Basei[4] · María Cecilia Cábana[5] · Silvio R. F. Vlach[4] · Martín Arce[6] · Martín Parada[6]

Received: 3 March 2020 / Accepted: 23 September 2020 / Published online: 9 October 2020

Abstract

The temporal and spatial relationships between polyphase folding and faulting, regional metamorphism, and granitoids intrusions are discussed for the low-grade basement rocks of the El Jagüelito Formation from the eastern North Patagonian Massif, Argentina, at the inferred western Gondwana margin. As a result of the tectonometamorphic and magmatic events, a late Cambrian-early Ordovician orogenic belt is revealed in northern Patagonia and shall be named the Transpatagonian orogen. It is an NW–SE-trending belt traced from the extra-Andean North Patagonian Cordillera region via the eastern North Patagonian Massif up to the Atlantic coast in the east. The early Paleozoic Transpatagonian orogen is the result of compressional tectonics, also showing a significant dextral shearing, and regional metamorphism leading to the development of a fold-and-thrust belt with an anticlockwise P–T–D-time path. The double-sided orogen is divided into three tectonometamorphic zones bounded by NW–SE trending major faults. Regional comparisons of our results in the present contribution together with available geological data, allow characterizing the orogen as part of a paired metamorphic belt system, with an outboard low-P/high-T belt (northern Patagonia terrane) and a parallel, inboard medium-P/T belt of Barrowian type (Famatinian Orogen on Gondwana margin), respectively. They are juxtaposed tectonically along with the contact of the suture Huincul Fault Zone. The Transpatagonian orogen was implanted along the southernmost Gondwana margin during the final stages of the supercontinent assembly in the early Paleozoic. The tectonism of the Permian Gondwanide orogeny reworked the Transpatagonian orogen.

Keywords Fold-and-thrust belt · Low-grade metamorphism · Anti-clockwise P–T-time path · Early Paleozoic · Patagonia

Introduction

After the early Neoproterozoic break-up of the Rodinia supercontinent, the dispersed Mesoproterozoic crustal fragments were gradually reassembled to form Gondwana by the Ediacaran-early Paleozoic. During the assembly, the Terra Australis orogenic belt implanted along the (paleo) Pacific-Iapetus oceanic margin of Gondwana between Australia and South America (Cawood 2005). The orogen has a protracted history of ongoing subduction along with inboard continental margin sequences that occur, outboard of which lay a series of Gondwanan parautochthonous and Laurentian allochthonous terrains (Schmitt et al. 2018).

In South America (28°–39°S region, present latitudes), the Laurentian-derived Mesoproterozoic terranes record the successive tectonic and metamorphic effects of their subsequent accretion against the western Gondwana margin, concomitantly with the final assembly of the continent in the early Paleozoic (Cawood 2005; Cawood et al. 2007; Oriolo et al. 2017; Rapalini et al. 2018, among many others). The Gondwana border was the locus of a superposed westward succession of orogenies, west of the Paleoproterozoic Río de la Plata craton (Fig. 1): (1) *the Pampean orogeny* (latest Neoproterozoic-middle Cambrian, Aceñolaza and Toselli 1976), partly involved in the Pampia terrane (Ramos and Vujovich 1993; Ramos et al. 2010) and evidenced primarily in the Sierras Pampeanas of Córdoba (e.g., Rapela et al. 1998; Siegesmund et al. 2009; von Gosen and Prozzi 2010; Casquet et al. 2018), and (2) *the Famatinian orogeny* (late

Electronic supplementary material The online version of this article (https://doi.org/10.1007/s00531-020-01939-0) contains supplementary material, which is available to authorized users.

✉ Pablo D. González
pdgonzalez@unrn.edu.ar

Extended author information available on the last page of the article

Fig. 1 Regional map of South America showing the locations of Patagonian basement blocks, the accreted terranes to the west of the Río de la Plata craton, and the Pampean-Famatinian belts on Gondwana margin. Solid red lines are major terrane boundaries. In Patagonia, the igneous-metamorphic basement areas of the eastern North Patagonian Massif are (1) Nahuel Niyeu-Aguada Cecilio; (2) Sierra Pailemán-Mina Gonzalito; (3) Sierra Grande-Playas Doradas. The base map is a colour shaded-relief image freely downloaded from https://creativecommons.org/licenses/by-sa/3.0/deed.es. The location of Fig. 2a is shown by rectangle. NPM in overview map: North Patagonian Massif

Cambrian-Devonian, Aceñolaza and Toselli 1976), overprinting the previous Pampean orogen in all the Sierras Pampeanas (e.g., Pankhurst et al. 2000; Sato et al. 2003; Ramos 2018) and the Chadileuvú Block (Tickyj et al. 2002; Chernicoff et al. 2010).

The *Famatinian orogeny* is associated with the proposed successive collisions of Laurentian-derived Cuyania and Chilenia terranes to the west, in the Ordovician and Devonian, respectively (Ramos 1988,2004; Ramos et al. 1986). The Ordovician is the climax of the main tectonothermal phase of the Famatinian orogeny responsible for delineating the most significant pre-Andean orogenic features (e.g., Sato et al. 2003; Varela et al. 2011a). As a result, a conspicuous N–S trending *Famatinian Orogenic Belt* involved arc magmatism, pervasive deformation, and low-to-high grade regional metamorphism, overprinting both the autochthonous Gondwana border and the allochthonous Cuyania terrane (Fig. 1).

The southern extension of the Famatinian orogen through Patagonia (south of 39°S) is questionable and a matter of debate due to the controversial origin and evolution of the early Paleozoic igneous and metamorphic basement rocks of the North Patagonian Massif. It has been considered as either related to the collision of an allochthonous terrane (Ramos 1984) or to be part of the autochthonous Gondwana margin (Dalla Salda et al. 1992), and even developed in a parautochtonous terrane (González et al. 2018).

The focus of this paper is to characterize the polyphasic deformational structures of the early Paleozoic basement rocks from eastern North Patagonian Massif (Sierra Grande-Playas Doradas area, 41° 33′ S–65° 15′ W, Fig. 1). The associated metamorphic features are recorded by mineral assemblages-reaction textures combined with Kübler/Árkai indices and chlorite thermometry. Regional comparisons with geotectonic implications are provided to assess whether the eastern North Patagonian basement belongs to the autochthonous Famatinian Orogen or is involved in an independent orogenic belt. Throughout the text, the ICS International Chronostratigraphic Chart of Cohen et al. (2013, updated) has been used.

The geotectonic setting of Patagonia

In extra-Andean Patagonia south of the Colorado River (~39°S), the occurrence of the above suggested geotectonic framework of the Sierras Pampeanas-Chadileuvú segment (28°–39° S), outlined by a westward sequence of early Paleozoic orogenic belts and accreted terranes is unclear.

The basement rocks belong to a composite continental crustal segment divided into *North Patagonian Massif* and *Deseado Massif*, in the north and south, respectively, along with the subsurface basement of the *Magellan basin* representing either a southern extension of the Deseado Massif or an independent continental block. The North Patagonian Massif is bounded on the northern and southern sides by the Cretaceous Colorado and San Jorge basins, respectively. In contrast, the coeval Magellan basin separates the south side of the Deseado Massif from their subsurface basement block to the south (Fig. 1).

Regarding the geotectonic setting, on the one hand, Ramos (1984,2008) proposed that entire Patagonia (North Patagonian and Deseado massifs) is an allochthonous (exotic) terrane that collided with the southwestern Gondwana margin in late Paleozoic. The Patagonia terrane would not share the same distinctive early Paleozoic geologic history of the surrounding areas and, therefore, the Famatinian orogen would have no continuity in Patagonia. The suture between the Patagonia terrane and the autochthonous

Gondwana margin would be located around 39° S, at the subsurface basement of the Colorado basin, along the *Huincul Fault Zone* (Turner and Baldis 1978). Most of the lithological, structural, geophysical, and magmatic evidence (Chernicoff and Zappettini 2004; Kostadinoff et al. 2005; Ramos 2008; von Gosen 2002, 2003; Ramos and Naipauer 2014, among others) argues in support to the Ramos (1984) allochthonous model.

On the other hand, Forsythe (1982) and Dalla Salda et al. (1992, 1993) interpreted Patagonia as part of South America since early Paleozoic times, considering the striking similarities of the lithologies, tectonometamorphic and magmatic features with the Sierras Pampeanas. According to this scheme the early Paleozoic basement units of Patagonia would be considered correlative equivalents of the Sierras Pampeanas-Chadileuvú Block basement complexes, also belonging to the same continental crust and sharing the same geological processes (González et al. 2002; Gregori et al. 2008; Pankhurst et al. 2014; among others). Detrital zircon patterns of meta-sedimentary rocks from Patagonia have striking similarities to those of the Sierras Pampeanas and, therefore, the age spectra were also considered a key correlation feature between both regions (Pankhurst et al. 2006; Rapalini et al. 2013; Rapela et al. 2016; Greco et al. 2017). Most of the geochronological, geochemical, isotopic, and petrological constraints focus on the above-suggested idea that Cambrian and Ordovician granites of northern Patagonia represent the southern continuation of the Pampean and Famatinian orogenic belts, respectively (Pankhurst et al. 2006, 2014; Gregori et al. 2008; Greco et al. 2017). However, the Cambrian plutonic rocks are now found to the west of the Ordovician plutons, and this contrasts with the inverse spatial arrangement of the Pampean and Famatinian belts of the Sierras Pampeanas. Besides, the Laurentian-derived "Grenvillian age" rocks are lacking to the west of the Cambro-Ordovician basement (Fig. 2).

Considering the contrasting autochthonous and allochthonous geodynamic models for Patagonia, new insights into the origin and evolution of the Cambro-Ordovician igneous and metamorphic basement deal with the eastern North Patagonian Massif as a parautochthonous terrane emerged as the Cambrian conjugate margin of the Pensacola-Queen Maud-Ellsworth-Whitmore Mountains region in East Antarctica (Ramos and Naipauer 2014; González et al. 2018). It was detached and transferred from East to West Gondwana, and then collided against the southernmost Gondwana margin of South America. In this geotectonic scenario, the eastern North Patagonian Massif is one element in the collage of outboard parautochthonous terranes reassembled during the final amalgamation of the supercontinent by the early Paleozoic. Although many lines of geological evidence point to a late Paleozoic time of Patagonia collision with South America (Ramos 2008; von Gosen 2003; Pankhurst et al. 2006; Ramos and Naipauer 2014), it could have occurred earlier in the Ordovician (González et al. 2018). The orogenesis involved in that collision is somewhat synchronous with the Famatinian orogeny of the Sierras Pampeanas-Chadileuvú Block, and its study falls within the scope of this contribution.

Lithological units

In the eastern North Patagonian Massif, the igneous-metamorphic basement exposures are isolated and distributed in a NW–SE corridor along with three distinctive areas, i.e., Nahuel Niyeu-Aguada Cecilio, Sierra Pailemán-Mina Gonzalito, and Sierra Grande-Playas Doradas areas (Fig. 1). Although they are geographically disconnected from each other, a regional geological correlation has been proposed among them, resulting from a common geological history. Critical correlative lithostratigraphic units include the low-grade Nahuel Niyeu and El Jagüelito formations and the high-grade Mina Gonzalito and Yaminué complexes, respectively (Ramos 1975; Caminos and Llambías 1984; Giacosa 1999). Likewise, the deformed and undeformed granitoid, i.e., the Tardugno Granodiorite (Caminos et al. 2001), Valcheta Granite (Gozalvez 2009), and Punta Sierra Plutonic Complex (Busteros et al. 1998) are comparable magmatic units (Fig. 2).

Stratigraphic, paleontological, structural, and U–Pb age constraints suggest mostly Cambrian deposition ages for the volcano-sedimentary protoliths, succeeded by early Paleozoic tectonometamorphic events, and Cambrian-Ordovician plutonism (von Gosen 2002, 2003; Pankhurst et al. 2006, 2014; Rapalini et al. 2010, 2013; Greco et al. 2015, 2017; González et al. 2008a, 2010, 2011a, 2018). Table 1 summarizes tectonometamorphic features of the correlating basement units of the eastern North Patagonian Massif.

Finally, the Cambro-Ordovician basement is unconformably covered by sandstones and quartzites of the Upper Ordovician–Silurian Sierra Grande Formation (Fig. 2). It indicates a significant hiatus, which includes substantial uplift, erosion, and leveling of the basement. Then, the structures affecting the Sierra Grande Formation are younger than, at least, Siluro-Devonian and related to the orogenic effects of the late Paleozoic Gondwanide orogeny (Giacosa 2001; von Gosen 2002).

Non-deformed granitoid plutons of the Gondwanide magmatic cycle intruded the basement and the sedimentary cover (e.g., Pailemán Plutonic Complex and equivalents). A continental-scale rhyolitic ignimbrite plateau of the Jurassic Marifil Complex, Cretaceous-Quaternary sedimentary rocks, and Cenozoic basaltic lava flows of the Meseta de Somuncura unconformably cover all the previously described units (Caminos et al. 2001; Busteros et al. 1998).

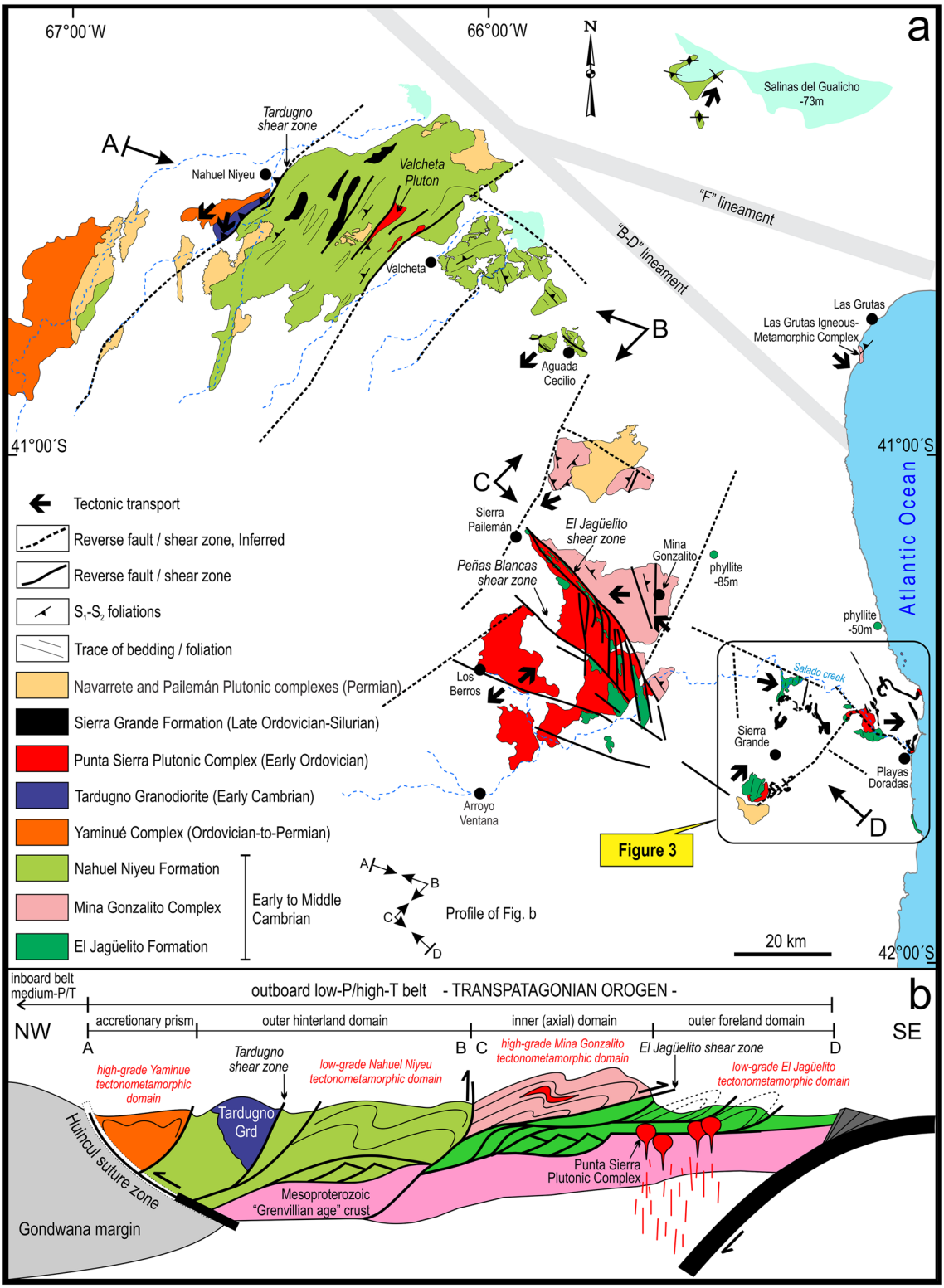

Fig. 2 **a** Geological sketch map of the Cambro-Ordovician igneous-metamorphic basement outcrops in the eastern North Patagonian Massif. The location of map is shown in Fig. 1. Rectangle shows the location of map of Fig. 3. **b** NW–SE trending regional geological cross-section of the Transpatagonian Orogen exhibiting the primary internal divisions and major boundaries. Profile location is shown in map (**a**). Tectonic transports and subsurface structure are based on surface geology cited in the text

Table 1 Geological synthesis of the igneous-metamorphic basement units in the eastern North Patagonian Massif

			Nahuel Niyeu Formation	Mina Gonzalito Complex	El Jagüelito Formation
Late Paleozoic Gondwanide orogeny	Metamorphism		M_2 greenschist facies (chlorite zone) regional metamorphism Age: c. 265 Ma	M_3: amphibolite facies (sillimanite grade) shear zone metamorphism Age: c. 257 Ma	M_2 greenschist facies shear zone metamorphism Age: c. 260 Ma
	Structures/Deformation event		WNW–ESE fabric superposed to D_1–D_2, S_3 crenulation cleavage, F_3 folds, high-angle reverse faults; tectonic transport to the SW. D_3	NW–SE to N–S ductile shear zones (e.g., El Jagüelito shear zone) with mylonitic foliation, F_3 folds. D_3	NW–SE trending S_2 crenulation cleavage and kink bands, NE-directed thrusts, E–W to WNW–ESE brittle-ductile shear zones. D_2
Early Paleozoic orogeny	Metamorphism		M_1 greenchist facies (biotite zone) regional metamorphism Age: 490–473 Ma (zircon rims)	M_{1-2} amphibolite facies (garnet and sillimanite zones) regional metamorphism Age: 472–470 Ma (zircon rims)	M_1 greenchist facies (chlorite zone) regional metamorphism Age: 493–474 Ma (zircon rims)
	Structures/Deformation event		Penetrative WNW–ESE fabric, S_1–S_2 axial plane cleavages, F_1–F_2 coaxial folds, tectonic transport blurred by the overprint of younger deformation events. D_1–D_2	Penetrative NNW–SSE to NW–SE fabric, S_1–S_2 axial plane foliations, F_1–F_2 coaxial folds, tectonic transport to the WSW-SW. D_1–D_2	Penetrative N–S to NNE–SSW fabric, S_1 axial plane cleavage, F_1 folds, high-angle reverse faults, tectonic transport to the E. D_1
Magmatic arc/back-arc system	Lithology		metagreywacke, phyllite, slate; minor metasandstone, granule metaconglomerate, metatuff, metapillow-basalt, andesite	paragneiss, amphibolite, micaschist; minor marble, orthogneiss	slate, phyllite, metagreywacke, minor metaconglomerate, meta K-bentonite, metaignimbrite, acidic lavas
	Protoliths	magmatic crystallization age (Ma)	mafic-to-felsic composite sill: 513	granodioritic orthogneiss: 492	tuffs, ignimbrite: 533, 529, 515
		maximum depositional age (Ma)	sandstones: 516, 515, 507	paragneisses: 540, 525 marbles: 550–510	conglomerate: 510 fossils: 521–513 greywackes: 533–515

Nahuel Niyeu Formation: Caminos et al. (2001); Chernicoff and Caminos (1996a, b); von Gosen (2003); Pankhurst et al. (2006); Rapalini et al. (2013); Greco et al. (2015, 2017). *El Jagüelito Formation*: Ramos (1975); Giacosa (1987); Busteros et al. (1998); Giacosa and Paredes (2001); von Gosen (2002); González et al. (2008a, b, c, 2013, 2014, 2018). *Mina Gonzalito Complex*: Ramos (1975); Giacosa (1999); Busteros et al. (1998); Pankhurst et al. (2006); González et al. (2008b), Varela et al. (2011b, 2014), Greco et al. (2014)

Nahuel Niyeu-Aguada Cecilio area

The Nahuel Niyeu Formation consists of alternating phyllite and metagreywacke, with minor metasandstone, granule metaconglomerate, and diabase sills (Chernicoff and Caminos 1996a; Caminos et al. 2001; Giacosa 1999). Intercalations of (meta-) tuffs, pillow-basalts, and andesite lava flows have also been described within the same sequence. U–Pb zircon data constrained the deposition of the volcano-sedimentary pile and diabase magmatic crystallization to the 516–507 time interval (Pankhurst et al. 2006; Rapalini et al. 2013; Greco et al. 2015, 2017). D_1–D_2 tectonometamorphic events are pre-to-syn-Lower Ordovician, as is constrained by the intrusion of the Ordovician Punta Sierra Plutonic Complex into deformed-metamorphosed rocks, and by U–Pb overgrowths in outer rims of detrital zircons yielding 490–473 Ma (Pankhurst et al. 2006; Rapallini et al. 2013; Greco et al. 2017), though younger Gondwanide ages have also been informed (Table 1).

The NE-SW trending and NW-dipping Tardugno shear zone and Nahuel Niyeu Thrust Sheet juxtaposed the Yaminué Complex against the Nahuel Niyeu Formation tectonically. S to SW-directed thrusting accompanied progressive deformation (Chernicoff and Caminos 1996b; von Gosen 2003).

The Yaminué Complex consists mainly of granodioritic-granitic orthogneiss and minor schist, paragneiss, marble, and amphibolite (Caminos et al. 2001). U–Pb age constraints of igneous protoliths reveal significant magmatic activity at 300–280 Ma (Pankhurst et al. 2006), 260–250 Ma (Basei et al. 2002; Chernicoff et al. 2013; Pankhurst et al. 2014, Martínez Dopico et al. 2017), and minor at ~ 467 Ma (Rapalini et al. 2013). U–Pb detrital zircon maximum depositional ages of 395 and 375 Ma are recorded to sedimentary protoliths (Chernicoff et al. 2013; Martínez Dopico et al. 2017). Although the main U–Pb age constraints allow assigning the polyphase deformation-metamorphism to Permian Gondwanide orogeny (Llambías et al. 2002; von Gosen 2003), the age of 467 Ma reveals the existence of relics of Ordovician tectonometamorphic events.

Mina Gonzalito-Sierra Pailemán area

The high-grade Mina Gonzalito Complex and the low-grade El Jagüelito Formation (Ramos 1975; Busteros et al. 1998; Giacosa 1999) are included as pendants into the Peñas Blancas and La Laguna granitic plutons belonging to the Ordovician Punta Sierra Plutonic Complex (González et al. 2008b; Varela et al. 2011b). The Mina Gonzalito Complex has been considered as the higher grade metamorphic equivalent of the lower grade Nahuel Niyeu-El Jagüelito formations (Caminos and Llambías 1984; Giacosa 1999), later sustained by U–Pb detrital zircon provenance studies (Pankhurst et al. 2006; Greco et al. 2014, 2017).

The Mina Gonzalito Complex is composed of paragneiss, amphibolite, micaschist, and migmatite, and minor intercalations of marble, meta-volcanic rock, and foliated orthogneiss. U–Pb detrital zircon data of 540–515 Ma and a mean $^{87}Sr/^{86}Sr$ ratio of 0.708730 ± 0.000285 from paragneisses and marbles, respectively, allow constraining the deposition of sedimentary protoliths to Ediacaran-Stage 4 time interval (Pankhurst et al. 2006; Greco et al. 2014; Varela et al. 2014). Overgrowths in outer rims of detrital zircons from the same paragneisses point to a 472–470 Ma age of the amphibolite facies metamorphism-ductile deformation (D_2–M_2, Table 1). A D_1-M_1 event older than Furongian is indicated by the pre-D_2 intrusion of a granodioritic pluton at ~ 492 Ma (Varela et al. 2011b). Syn-D_2–M_2 partial melting of pelites is coeval to the intrusion of syn-tectonic leucogranite phacoliths and dikes (Giacosa 1999; González et al. 2008b).

A NW–SE trending, westward-dipping and ~ 30 km wide mylonitic belt of the El Jagüelito, Peñas Blancas, and La Laguna shear zones, juxtaposed strips of the El Jagüelito Formation and Peñas Blancas pluton against the western contact of the Mina Gonzalito Complex tectonically (Fig. 2). Although SW-directed tectonic transports have been assigned to late Paleozoic tectonics (Giacosa 2001; von Gosen 2002; D_3 in Table 1), the belt formation can be of early Paleozoic age and later reactivated during Gondwanide orogeny (Giacosa 2020).

Sierra Grande-Playas Doradas area

The basement stratigraphy in this area consists of the El Jagüelito Formation intruded by the Punta Sierra Plutonic Complex (Figs. 2, 3). The El Jagüelito Formation is predominantly composed of slate, phyllite and metagreywacke, and minor metaconglomerate and mafic igneous rock. (Meta-) felsic lava flows, K bentonites, and ignimbrites are also interbedded as part of the volcano-sedimentary sequence (González et al. 2018). The volcano-sedimentary protoliths are assigned to the early-middle Cambrian according to original stratigraphic features (Busteros et al. 1998), a strontium isotopic record (Varela et al. 2014), trace and Archeocyath fossils (González et al. 2002, 2010), and U–Pb zircon ages (Pankhurst et al. 2006; González et al. 2018; Table 1). The chronologic sequence of deformational structures and correlated metamorphic features affecting the unit are presented below (Sects. 4 and 5).

Igneous activity

The Cambrian and Ordovician plutonism occur as the Tardugno Granodiorite and the Punta Sierra Plutonic Complex, respectively (Fig. 2). The Tardugno Granodiorite is

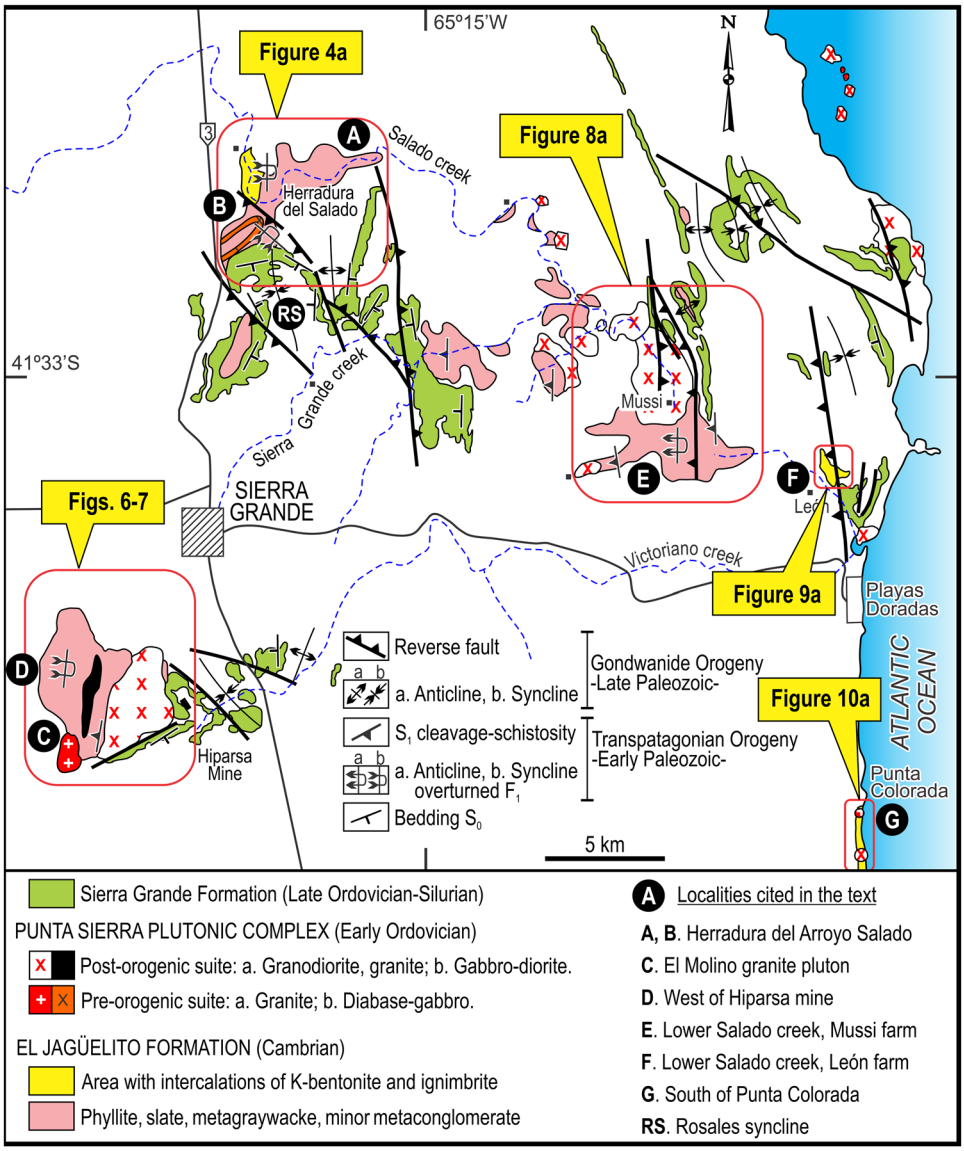

Fig. 3 Geological sketch map of the igneous-metamorphic basement rocks and the sedimentary cover in the Sierra Grande-Playas Doradas area. For location of map, see Fig. 2a. The selected study areas are shown by rectangles (maps of Figs. 4a, 6, 8a, 9a, and 10a) and are described in the text

composed of foliated porphyritic granodiorite and mylonite, and minor granitic orthogneiss and amphibolite (Chernicoff and Caminos 1996a; b). It intrudes into the Yaminué Complex, and in turn, they are juxtaposed against the Nahuel Niyeu Formation tectonically, along the Tardugno shear zone (Caminos et al. 2001; von Gosen 2003). U–Pb ages ranging from 529 to 522 Ma constrained the magmatic crystallization to Terreneuvian (Rapalini et al. 2013; Pankhurst et al. 2014).

The Punta Sierra Plutonic Complex has been divided into *pre-*, *syn-*, and *post-orogenic suites*, based on intrusive features concerning the tectonometamorphic events (González et al. 2020). The pre-orogenic granitoid plutons intruded the undeformed protoliths of the El Jagüelito Formation before the deformation and metamorphism took place (Fig. 3). They are bimodal (granite and gabbro-diorite) and share the same penetrative foliation and low-grade metamorphism of the (meta-) pelites and psammites.

The syn-orogenic Tapera and María Teresa phacoliths and a swarm of longitudinal dikes composed of S-type granitoids are emplaced parallel along the folded fabric of the Mina Gonzalito Complex. They intruded synchronously with the main tectonometamorphic event.

The post-orogenic plutons are ubiquitous in the three basement areas, ranging in composition from granodiorites/granites to tonalites/quartz diorites (Fig. 2). They cut with sharp contacts the penetrative fabrics of the Nahuel Niyeu and El Jagüelito formations, including pendants of these country rocks.

Available U–Pb zircon data indicate that the magmatic crystallization range mostly between 476 and 462 Ma, with one age of 492 Ma (Varela et al. 1998, 2008, 2011b;

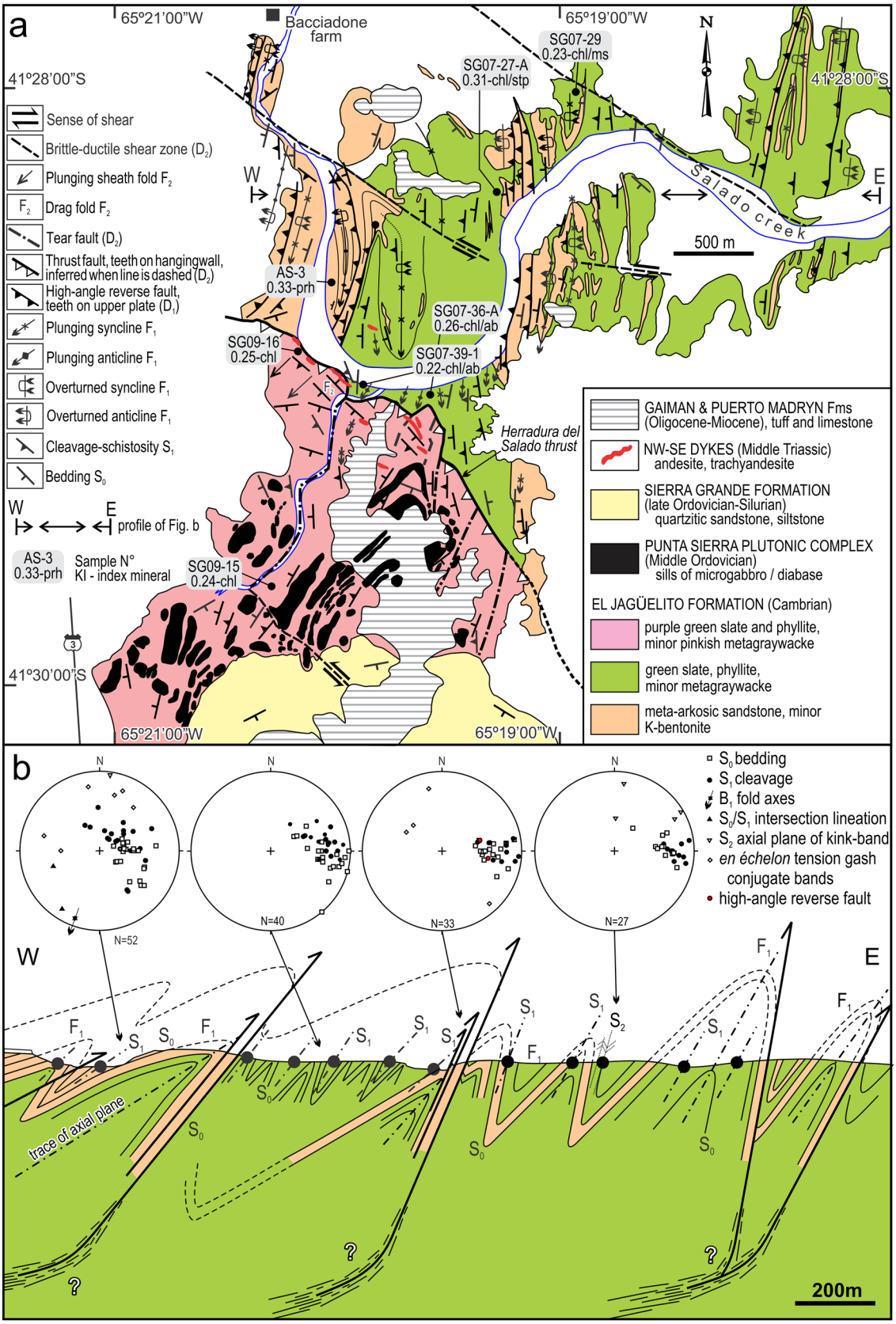
a
65°21'00"W
Bacciadone farm
65°19'00"W
41°28'00"S
41°30'00"S
N
Sense of shear
Brittle-ductile shear zone (D2)
Plunging sheath fold F2
Drag fold F2
Tear fault (D2)
Thrust fault, teeth on hangingwall, inferred when line is dashed (D2)
High-angle reverse fault, teeth on upper plate (D1)
Plunging syncline F1
Plunging anticline F1
Overturned syncline F1
Overturned anticline F1
Cleavage-schistosity S1
Bedding S0
W
E
profile of Fig. b
AS-3 0.33-prh
Sample N°
KI - index mineral
SG09-15 0.24-chl
SG09-16 0.25-chl
AS-3 0.33-prh
SG07-27-A 0.31-chl/stp
SG07-29 0.23-chl/ms
SG07-36-A 0.26-chl/ab
SG07-39-1 0.22-chl/ab
Herradura del Salado thrust
Salado creek
500 m
GAIMAN & PUERTO MADRYN Fms (Oligocene-Miocene), tuff and limestone
NW-SE DYKES (Middle Triassic) andesite, trachyandesite
SIERRA GRANDE FORMATION (late Ordovician-Silurian) quartzitic sandstone, siltstone
PUNTA SIERRA PLUTONIC COMPLEX (Middle Ordovician) sills of microgabbro / diabase
EL JAGÜELITO FORMATION (Cambrian)
purple green slate and phyllite, minor pinkish metagraywacke
green slate, phyllite, minor metagraywacke
meta-arkosic sandstone, minor K-bentonite
b
S0 bedding
S1 cleavage
B1 fold axes
S0/S1 intersection lineation
S2 axial plane of kink-band
en échelon tension gash conjugate bands
high-angle reverse fault
N=52
N=40
N=33
N=27
trace of axial plane
200m

◂**Fig. 4** **a** Geological map of the El Jagüelito Formation and the associated intrusions in the Herradura del Arroyo Salado area, based on field mapping. For the map location, see Fig. 3. **b** E–W trending geological cross-section exhibiting the D_1–D_2 structures of the basement. See the profile location in Fig. a. Stereoplots are lower hemisphere, equal-area projections of structural elements

Pankhurst et al. 2006). Despite the division based on the relationship between intrusive stages and orogenesis, the magmatic crystallizations of the suites overlap each other, revealing spatial and temporal synchronicity in pluton emplacement and orogenesis (González et al. 2020).

Structure of the El Jagüelito Formation and associated intrusions

D_1-deformation: the El Jagüelito fold-and-thrust belt

The major D_1 structure of the El Jagüelito Formation is the *El Jagüelito fold-and-thrust belt*. The cross-cutting relationships between S_0 and S_1 planes, the marker horizons to stratigraphic correlation, the way-up indicators, and the "S–M–Z" geometries of parasitic folds, among others, allow reconstructing the different limbs and hinge zones within regional domains of anticlines and synclines. During the belt formation and evolution, syn-metamorphic folding and thrusting are either coeval or folding precedes thrusting. According to the westward-dipping S_0–S_1 planes and fault surfaces, and the E-directed vergence of overturned folds F_1, the fold-and-thrust belt displays an eastward tectonic transport.

Herradura del Arroyo Salado

In this area (localities A–B, Fig. 3), strips of the El Jagüelito Formation are juxtaposed tectonically by a low-angle reverse fault D_2, that refolds the fabric D_1 (Fig. 4, González et al. 2011b). The unit consists mainly of slate, phyllite, and metagreywacke, alternating with (meta-) arkosic pumice sandstone/K-bentonite, and pre-orogenic gabbro-diabase sills in the northern footwall and southern hanging-wall blocks, respectively.

In the footwall, D_1-related structures of the fold-and-thrust belt are well-preserved, least transposed by D_2 shortening. Bedding S_0 is folded around an E-verging, overturned and tight F_1 synclinorium of around 750 m width and composed of meta-pelites (Fig. 4a). It comprises a succession of subordinate, asymmetric Z- and S-anticlines and synclines of decameter-scale on the western and eastern limbs, respectively. Along with them, S_0 is N–S to NNE–SSW trending and dips 65°–80° to the west, whereas S_1 axial plane cleavage is parallel to S_0 and dips 30°–60° to the west (Figs. 4b, 5a). N–S to NNE–SSW striking fold axes B_1 plunge ~ 40° to the south. The hinge of the synclinorium closes northward and southward; in the latter the NNE-SSW striking fold axis plunges less than 40° to the S-SSW. Open F_2 folds refold F_1 anticlines and synclines.

To the west and east, the synclinorium is flanked by overturned tight F_1 anticlines of decameter-scale consisting of alternating (meta-) arkosic sandstones and K-bentonites. S_0–S_1 planes are N–S to NNE–SSW trending and variably dipping to the west. S_1 cleavage planes display a convergent radiating fan pattern towards the core of the anticlines, and in the normal longer back limb dips steeper than the S_0, and in the overturned short forelimb shallower.

Reverse faults developed parallel to bedding can be considered as thrust faults, some ending along the strike of the strata. Asymmetric bending of layers also suggests that thrusts are part of fault-propagation folds above a basal thrust horizon (Fig. 5b, c). Fault planes strike ~ N–S with dips > 65° to the west. Striae on sandstone bed surfaces document eastward tectonic transport. In the inner arc of overturned forelimbs of anticlines, subsidiary high-angle reverse faults also formed as fold-accommodation faults.

West of Hiparsa Mine, Sierra Grande

In this area near Sierra Grande town (localities C–D, Fig. 3), the El Jagüelito Formation and the pre-orogenic El Molino pluton share the same D_1 structures (see also Sect. 4.2). The first consists of slate, phyllite, metagreywacke, hornfel, and minor intercalations of dacite-to-rhyolite and granule-to-cobble metaconglomerate lenses (Fig. 6). The volcano-sedimentary bedding S_0 is folded around E-verging, overturned tight F_1 synclines and anticlines (Fig. 7a). Tight-to-close F_1 folds with thickened hinge zones developed in most competent igneous bodies and metagreywackes, whereas closed similar folds in less competent slates and phyllites. The N–S to NNE–SSW trending S_0 bedding and S_1 cleavage dips to the west, between 65°–80° and lower angles of 30°–60°, respectively. S_1 displays a radiating convergent or divergent fan pattern. Late-D_1/pre-D_2 low-grade ductile shear zones also developed after folding/axial plane cleavage formation (Sect. 4.3.).

Lower Arroyo Salado creek, Mussi farm area

The El Jagüelito Formation (locality E, Fig. 3) comprises hornfels, schist, metagreywacke, slate, phyllite, and metasiltstone, and minor (meta-) K-bentonite, sandstone, and granule conglomerate (Fig. 8a). Before the intrusion of the post-orogenic Arroyo Salado pluton, the S_0 bedding was folded around E-verging, overturned F_1 synclines and anticlines

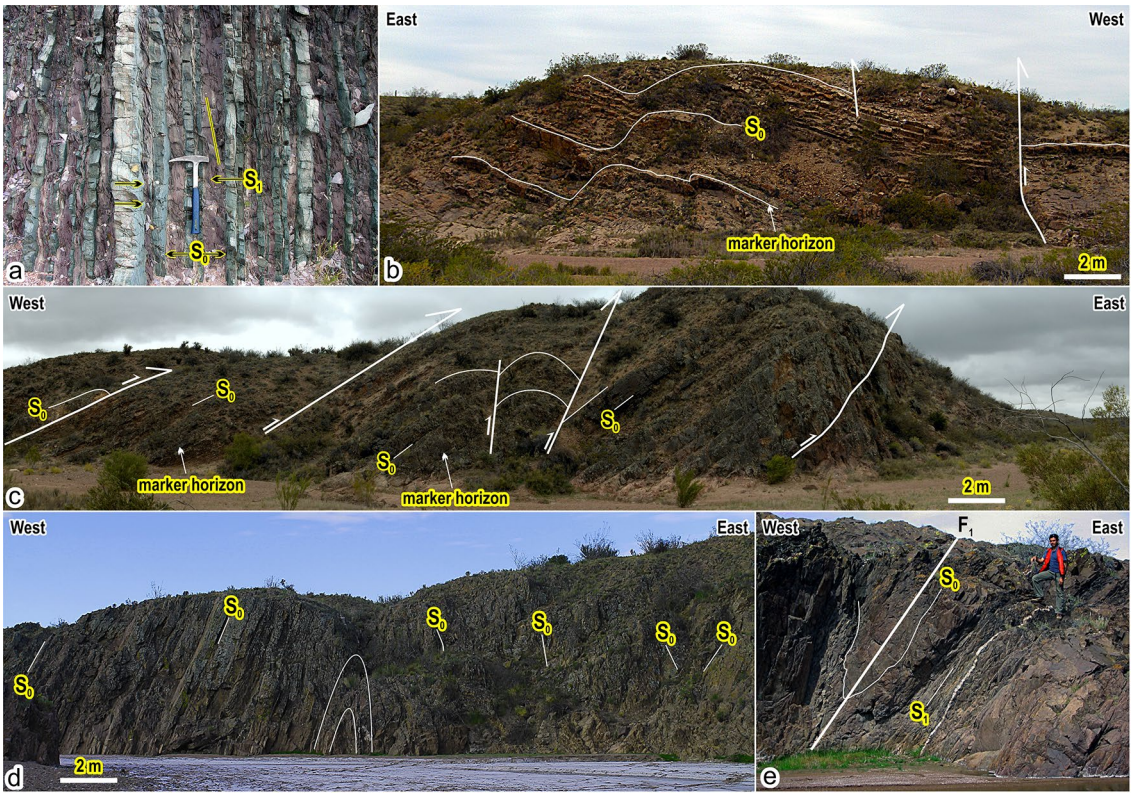

Fig. 5 Field view of D_1 structures in the El Jagüelito fold-and-thrust belt at Herradura del Salado (**a**–**c**) and lower Arroyo Salado creek (Mussi farm) areas (**d**, **e**). **a** Alternating beds of metagreywackes and slates exhibiting the S_0/S_1 structural relationship. Red arrows indicate ripple marks as way-up indicators on top of a metagreywacke bed. The sequence is younger towards the right side of the photograph. **b** Interlayered (meta-) arkosic sandstones (marker horizons) and K bentonites affected by fault-propagation folds. **c** High-angle reverse faults developed parallel to bedding S_0. Subsidiary high-angle reverse faults develop in the shortened inner arc of largely overturned anticlinal F_1 forelimb. **d** Alternating beds of metagreywackes and phyllites folded around E-verging, tight anticline-syncline F_1 of decameter-scale. **e** E-verging tight syncline F_1 of meter-scale exhibiting the S_0/S_1 structural relationship

along with parasitic Z- and S-folds on limbs (see also von Gosen 2002).

The structural pattern of the F_1 folds changes eastward in symmetry, tightness, and attitude, along the eastern margin of the pluton (Fig. 8b). Close to the intrusive contact, S_0 is folded around upright to steeply inclined tight to isoclinal F_1 folds. The N–S trending S_0 and S_1 planes dip to the west with > 85° and > 75°, respectively.

About 600 m east of the contact, S_0 is folded around overturned tight-to-close F_1 folds and dips 50°–70° to the west. The S_1 cleavage also dips to the west but at higher angles of 65°–75°. S_0–S_1 displays a general E-directed vergence. Finally, at around 2500 m to the east, the F_1 folds are symmetric, open and upright with hinge line plunging 35–55° to the south. The S_0 and fanning axial plane cleavage S_1 strike NNW-SSE and dip steeply to the east and west (Fig. 5d, e).

The changing structural pattern of the F_1 folds might be ascribed as effects of the local superposition of pluton emplacement-related deformation on folds already formed by D_1 deformation (e.g., Paterson et al. 1991). Stoping plus lateral wall-rock displacement by modification of pre-existing folds seems to be the most likely pluton emplacement mechanism in the already shallowly exhumed metamorphic rocks.

Lower Arroyo Salado creek, León farm area

The El Jagüelito Formation (locality F, Fig. 3) is composed of alternating (meta-) pumice sandstone and siltstone beds, a (meta-) ignimbrite stratum, and a felsic dome. A NE-SW trending normal fault dipping 66° to the SE is the main D_1-related structure of the area. The fault formed by hinge collapse of an F_1 syncline containing the competent meta-ignimbrite intercalated with incompetent meta-siltstones (Fig. 9a). In the footwall domain, S_0 is folded around a NNW-plunging and WSW-verging and overturned tight F_1 anticline. S_0–S_1 planes are NNW-SSE trending, dipping to the east at 60–65° and 65–76°, respectively (Fig. 9b). In the hanging wall domain, S_0 is folded around NW/NNW-plunging, near symmetric upright tight F_1 anticlines and synclines, with lack of a definite vergence. The NNW-SSE trending S_0 dips to the west and east 60–75°, whereas the

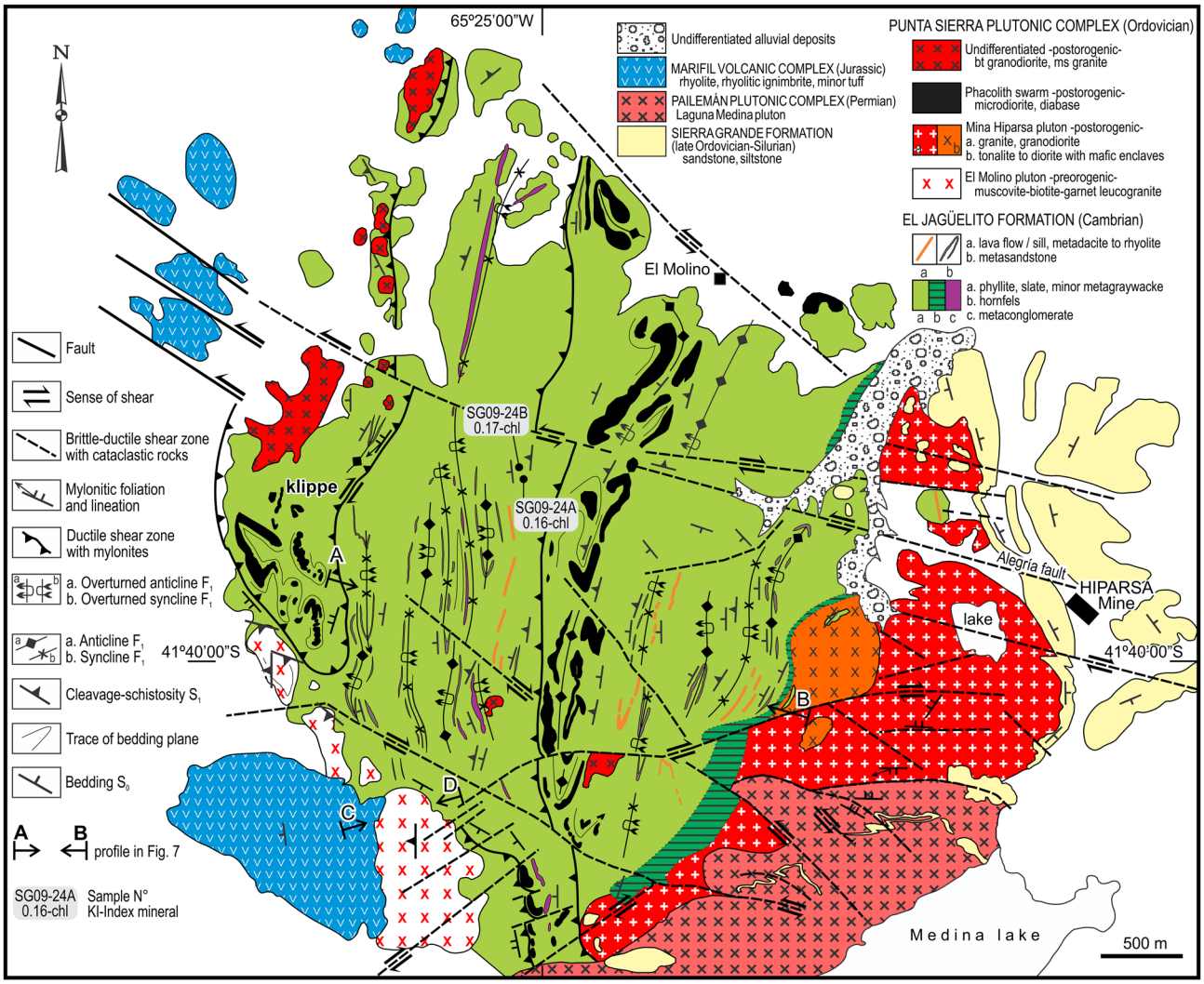

Fig. 6 Geological map of the El Jagüelito Formation and adjacent intrusions in the west of the Hiparsa Mine area, based on field mapping. For the map location, see Fig. 3

fanning axial plane cleavage S_1 dips ~ 80° to the west. The contrasting style of the vergence in both the footwall and the hanging wall domains remains unclear. There must have been a detachment horizon somewhere in the subsurface that enabled shortening by differential folding above. However, this thrusting must not lead to a general E-directed vergence in the folded block (e.g., Geiser 1988; Ferrill and Dunne 1989).

D_1-deformation of the pre-orogenic intrusive suite

The El Molino and San Pedro granitic plutons and the Herradura del Salado gabbroic sill swarm belong to the pre-orogenic igneous suite of the Punta Sierra Plutonic Complex. According to their emplacement histories, the bodies intruded into undeformed and non-metamorphosed protoliths of the El Jagüelito Formation (González et al. 2020; Fig. 3). Their original shapes and contact aureoles were modified by the deformation D_1 and regional metamorphism M_1, resulting in highly sheared borders and heterogeneously deformed inner zones.

The primary intrusive contact of the El Molino pluton and satellite granitic bodies with El Jagüelito Formation is sharp (Fig. 6). It follows roughly the S_0 bedding along the eastern side and crosscuts the S_0 planes along the northern side. A thin strip of hornfels with muscovite and biotite porphyroblasts developed along the eastern side in contact with a chilled margin of the granite.

In the El Molino granite, the N–S to NE–SW trending S_1 foliation dips 25°–50° to the southwest and is parallel to that of the country rocks. Locally, it exhibits thin ductile shear bands whit the L_1 stretching lineation plunging < 30° to the SW, comparable with the L_1 lineation of the country-rock

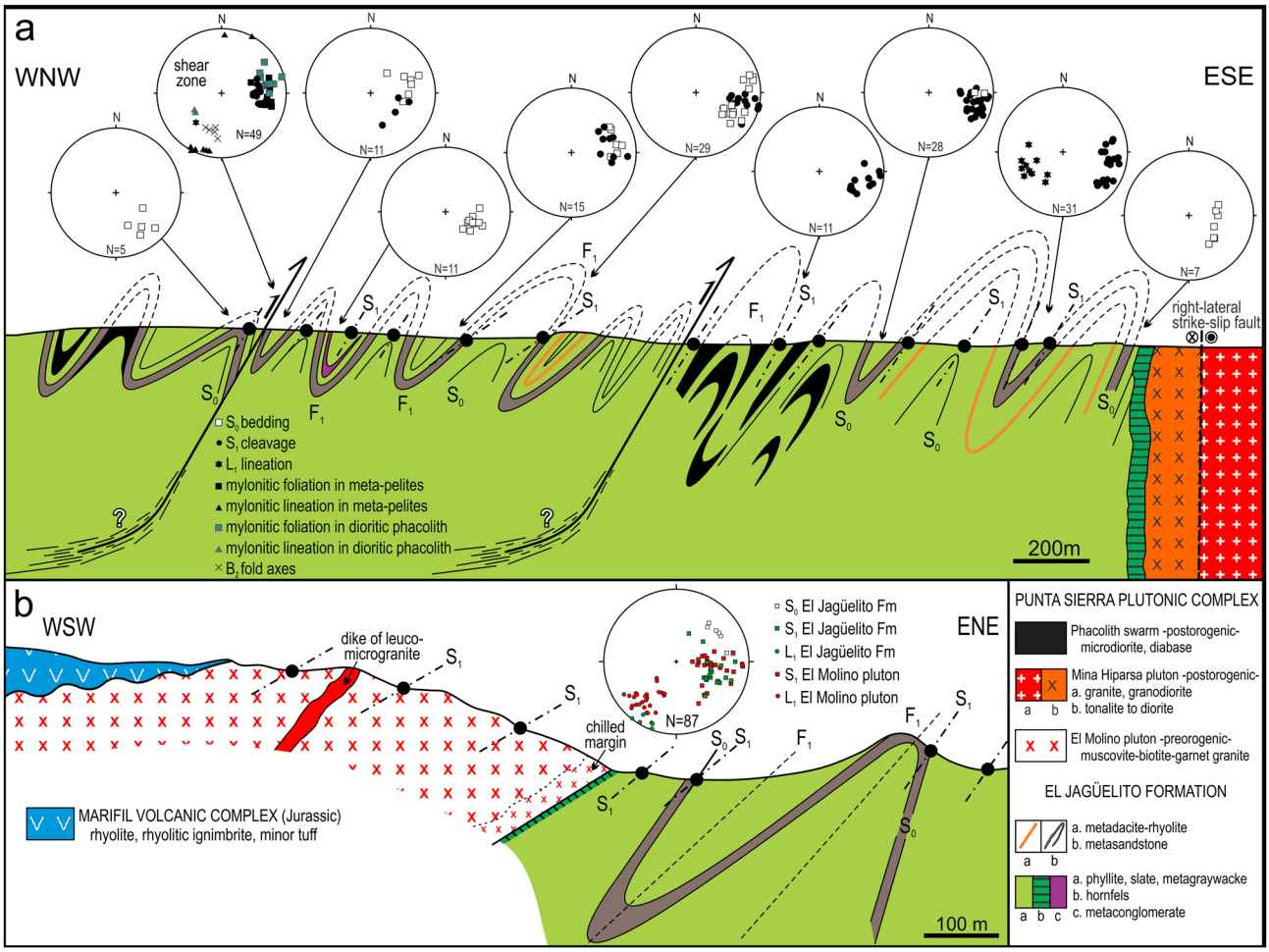

Fig. 7 **a**, **b** Geological cross-sections exhibiting the original stratigraphic and D_1–D_2 structural features among the El Jagüelito Formation and Punta Sierra Plutonic Complex, west of the Hiparsa mine area. For the profile location, see Figs. 3 and 6. Stereoplots are lower hemisphere, equal-area projections of structural elements

(Fig. 7b). Kinematic indicators suggest reverse dextral shearing toward the NNE.

The NE–SW trending Herradura del Salado swarm of micro-gabbro/diabase sills intruded parallel to the S_0 bedding planes of the El Jagüelito Formation (Figs. 3, 4). The sills incorporated pendants of the surrounding rocks, also revealing chilled margins on both contact surfaces. Thin strips of orange-red thermal oxidation aureoles, fine-grained hornfels, and porphyroblasts of andalusite were developed in the wall-rocks. As the main D_1-related structures, the sills and its contact aureoles are boudinaged along strike, also sharing the S_1 cleavage and tight F_1 folds of the country rocks. The NE–SW trending S_0 dips steeply to the west, whereas S_1 is also NNE–SSW to NE–SW trending and dips gently to the west. S_1 in the mafic rocks is rough, spaced, and discrete.

Late-D_1 to pre-D_2 deformation

Late-D_1 to pre-D_2 ductile and brittle-ductile shear zones developed shortly after the F_1 fold/S_1 axial plane cleavage formation. In the west of the Hiparsa mine, a set of N–S to NNE–SSW trending and west-dipping low-grade ductile shear zones cut pre-/post-orogenic bodies of the Punta Sierra Complex and the El Jagüelito Formation. They consist of strips of granitoid mylonites and phyllonites alternating with non-mylonitized phyllites/slates and granites. They are, in turn, displaced by right-lateral brittle-ductile strike-slip faults of the D_2 tectonic event (González et al. 2008a).

The westernmost shear zone in Fig. 6 is a narrow mylonitic belt of < 10 m width, associated with a sizeable klippe-like structure. In inner parts, S_0–S_1 planes of meta-pelites are affected by a N–S to NNE–SSW trending

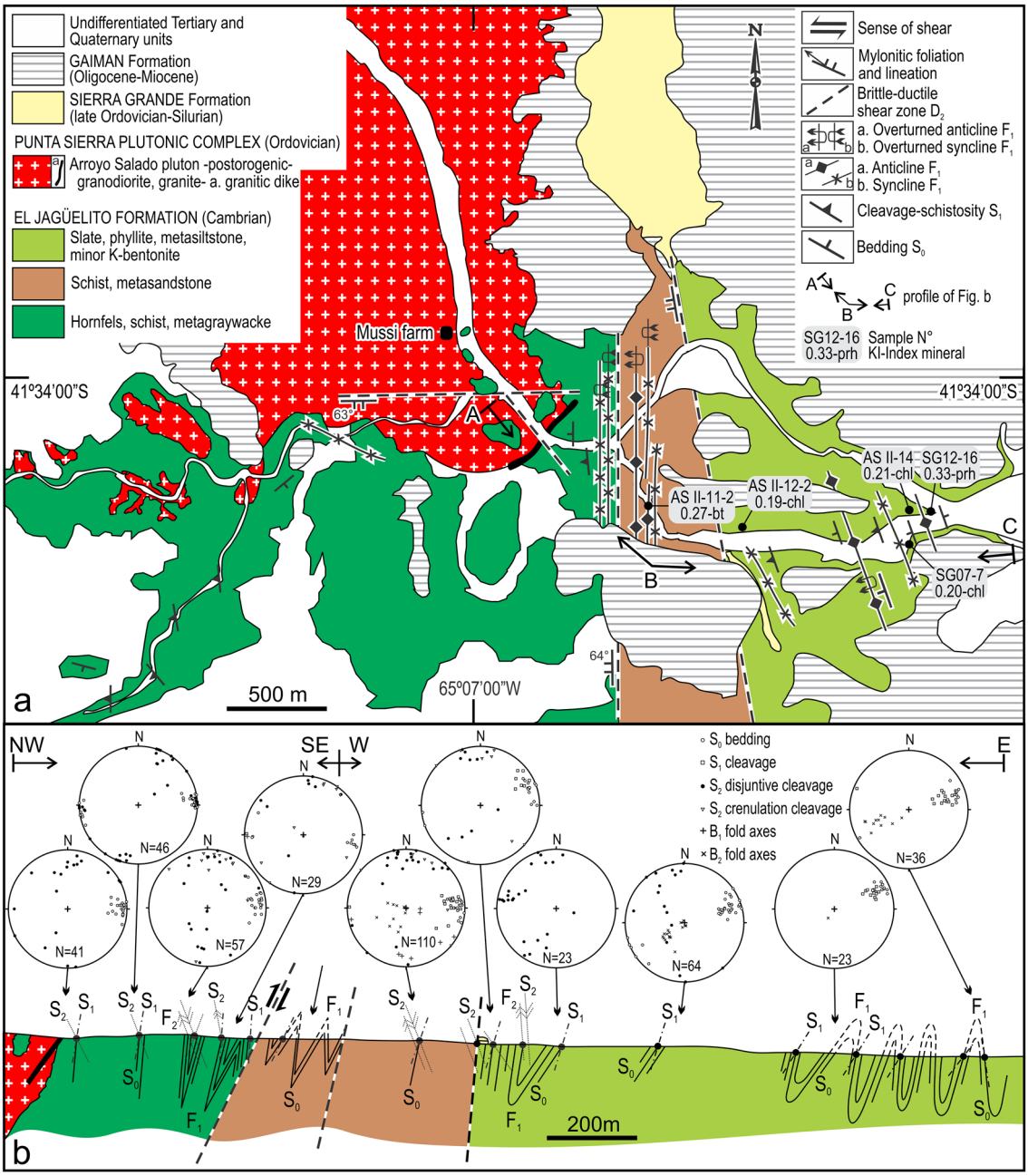

Fig. 8 **a** Geological map of the El Jagüelito Formation and the post-orogenic Arroyo Salado pluton in lower Arroyo Salado creek area, east of the Mussi farm, based on field mapping. For the map location, see Fig. 3. **b** Combined NW–SE to E–W trending geological profile exhibiting D_1–D_2 structures affecting the basement. See the profile location in Fig. a. Stereoplots are lower hemisphere, equal-area projections of structural elements

mylonitic foliation, dipping 60°–70° to the SW, and a mylonitic lineation plunging < 10° to the SSW (Fig. 7a, see the stereo plot of the "shear zone"). Mica fish and S/C fabrics indicate top-to-the NNE dextral sense of shear of the hanging-wall under ductile conditions, parallel to mylonitic lineation. In less mylonitized outer parts of the shear zone, the mylonitic foliation records continuous transitions into crenulation cleavage S_2, with fold axis F_2 plunging in the same way as the mylonitic lineation but with higher angles of 39°–45°.

A N–S trending strip with granitic mylonites and sheared leucogranite dikes of the San Pedro pluton is ~ 1200 m long and 100 m wide (locality G, Fig. 3). The pluton cuts the S_0 of the El Jagüelito Formation along the eastern margin with sharp contact, incorporating pendants with andalusite porphyroblasts. Along the western side, a N–S trending and west-dipping

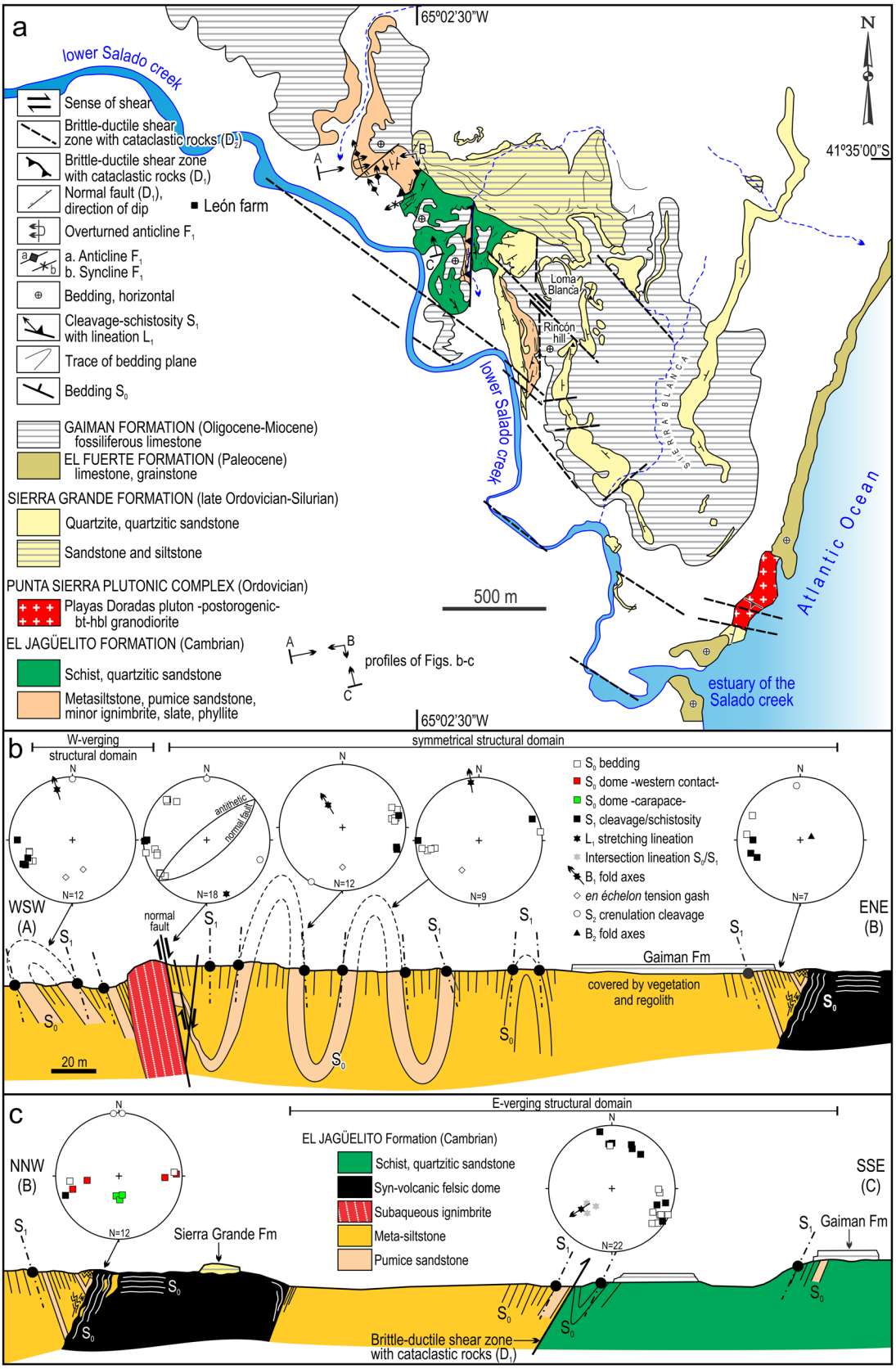
a
65°02'30"W
N
41°35'00"S
lower Salado creek
Sense of shear
Brittle-ductile shear zone with cataclastic rocks (D2)
Brittle-ductile shear zone with cataclastic rocks (D1)
Normal fault (D1), direction of dip
León farm
Overturned anticline F1
a. Anticline F1
b. Syncline F1
Bedding, horizontal
Cleavage-schistosity S1 with lineation L1
Trace of bedding plane
Bedding S0
GAIMAN FORMATION (Oligocene-Miocene)
fossiliferous limestone
EL FUERTE FORMATION (Paleocene)
limestone, grainstone
SIERRA GRANDE FORMATION (late Ordovician-Silurian)
Quartzite, quartzitic sandstone
Sandstone and siltstone
PUNTA SIERRA PLUTONIC COMPLEX (Ordovician)
Playas Doradas pluton -postorogenic- bt-hbl granodiorite
EL JAGÜELITO FORMATION (Cambrian)
Schist, quartzitic sandstone
Metasiltstone, pumice sandstone, minor ignimbrite, slate, phyllite
profiles of Figs. b-c
500 m
Loma Blanca
Rincón hill
SIERRA BLANCA
Atlantic Ocean
estuary of the Salado creek
b
W-verging structural domain
symmetrical structural domain
S0 bedding
S0 dome -western contact-
S0 dome -carapace-
S1 cleavage/schistosity
L1 stretching lineation
Intersection lineation S0/S1
B1 fold axes
en échelon tension gash
S2 crenulation cleavage
B2 fold axes
antithetic
normal fault
N=12
N=18
N=12
N=9
N=7
WSW (A)
ENE (B)
normal fault
Gaiman Fm
covered by vegetation and regolith
20 m
c
E-verging structural domain
EL JAGÜELITO Formation (Cambrian)
Schist, quartzitic sandstone
Syn-volcanic felsic dome
Subaqueous ignimbrite
Meta-siltstone
Pumice sandstone
N=12
N=22
NNW (B)
SSE (C)
Sierra Grande Fm
Gaiman Fm
Brittle-ductile shear zone with cataclastic rocks (D1)

◂**Fig. 9** **a** Geological map of the igneous-metamorphic basement and the overlying sedimentary cover in lower Arroyo Salado creek, close to the León farm area, based on field mapping. For the map location, see Fig. 3. **b**, **c** Combined WSW–ENE and NNW–SSE trending geological profile exhibiting the D_1–D_2 structural features. See the profile location in Fig. a. Stereoplots are lower hemisphere, equal-area projections of structural elements

ductile shear zone juxtaposed the pluton and (meta-) siltstones and sandstones of the El Jagüelito Formation tectonically. The shear zone is, in turn, displaced by left-lateral brittle-ductile strike-slip faults of the D_2 event (Fig. 10a).

In the pluton, a N–S trending mylonitic foliation dips 40°–55° to the west and is parallel to the S_1 foliation in less deformed parts. The mylonitic lineation of fibrolite plunges 40°–50° to SW (Fig. 10b). It records a continuous transition to S_1-L_1 of the country rocks in the east. The local development of S/C fabrics and asymmetric porphyroclasts indicate an extensional sinistral sense of shear toward the SW.

In the El Jagüelito Formation, the S_0 bedding planes are folded around overturned tight F_1 folds displaying an E-directed vergence. S_0 and S_1 planes strike N–S and dip to the west with 40°–60° and 50°–75°, respectively.

Shallow structural levels with brittle-ductile shear zones are exposed in the León farm area, at the Rincón hill (Fig. 9c). A NNE-SSW striking and WSW-dipping brittle-ductile shear zone juxtaposed strips of phyllites and schists tectonically in the west and east, respectively. It cuts parallel to S_0–S_1 planes of the metamorphic rocks with fault breccias and is, in turn, unconformably covered by sandstones and siltstones of the Sierra Grande Formation.

Microfabrics and metamorphism

Mineralogical, textural, and microstructural analyses of thin sections from slates and phyllites were carried out using standard optical microscopy. Online Resource 1 shows the data set of tectonometamorphic features and additional information can be found in González et al. (2011a, 2018). The petrographic study was complemented with 12 X-ray diffraction analyses of whole-rock powders and clay fraction (< 2 μm) of selected meta-pelites, performed at the DRX Laboratory of IIPG (CONICET-UNRN). Standard procedures for sample preparation, analytical conditions, and measurements of the Kübler/Árkai indices are summarized in Online Resource 2. Results of the petrographic and X-ray diffraction analyses are given in Table 2.

M_1-Mineral assemblages in the El Jagüelito Formation

The micro-folds and S_1 cleavage, overprinting the silty/argillaceous bedding S_0, resulted in the formation of quartz-feldspars microlithons (Q-F domains) bounded by cleavage M-domains (Fig. 11a). Quartz-chlorite-illite ± albite ± K-feldspar M_1 association defines S_1 planes, also containing stilpnomelane or biotite depending on the metamorphic grade. In the < 2 μm grain-size fraction of meta-pelites, illite and chlorite predominate in association with quartz, K-feldspar, and plagioclase. Primary mixed-layered smectite, montmorillonite, and kaolinite are also present as minor constituents of the clay fraction (Table 2).

In M-domains, pre-tectonic (pre-S_1) chlorite and white mica stacks developed as barrel-shaped porphyroblast aggregates with basal planes at high angles to S_1 cleavage, also with strain caps and shadows (Fig. 11b). Irregular interlayers of chlorite and illite/white mica also formed stacks, and rare prehnite or pumpellyite porphyroblasts can be noticed. Pre-S_1 veinlets consisting of quartz-albite-pumpellyite cross-cut the S_0 planes, whereas post-S_1 veinlets filled with zeolite-pumpellyite, intersects the S_1 cleavage planes (Fig. 11c, d).

M_1-Mineral assemblages and microstructures in the pre-orogenic intrusive suite

The igneous mineralogy of the El Molino pluton comprises K-feldspar, acidic plagioclase, quartz, biotite, muscovite, and scarce garnet. Accessory minerals are apatite, opaque minerals, zircon, and rare monazite. In the granitic mylonites, feldspar porphyroclasts preserve their igneous subhedral shapes partly though they are more commonly stretched, fragmented, or boudinaged into domino arrangements. Quartz is recrystallized into fine-grained, polygonal granoblastic aggregates following bands parallel to S_1 foliation. Muscovite (also biotite) fishes are consistent with dextral shearing (Fig. 11e). Shredding and thinning by cleavage slip of igneous mica are followed by abundant neocrystallization of sericite, chlorite, and biotite folia parallel to S_1 planes.

Igneous texture in micro-gabbro/diabases comprises basic plagioclase intergrown with clinopyroxene, Ti-bearing opaque minerals, skeletal olivine in more primitive gabbros, apatite, zircon, and granophyric quartz + K-feldspar. D_1 micro-structures are bent, kinked twin lamellae or tapered albite twins and undulose extinction in plagioclase, and deformation lamellae in clinopyroxene. Greenschists and weakly foliated meta-mafic rocks with aspect such as amphibolite exhibit lepidoblastic (schistose) and nematoblastic textures, respectively. M_1 assemblage alignment of chlorite-epidote-albite-tremolite/actinolite defines the S_1 schistosity, being also located as pseudomorphic replacement of the igneous minerals, and fillings of primary vugs-amygdales and post-S_1 veinlets (Fig. 11f).

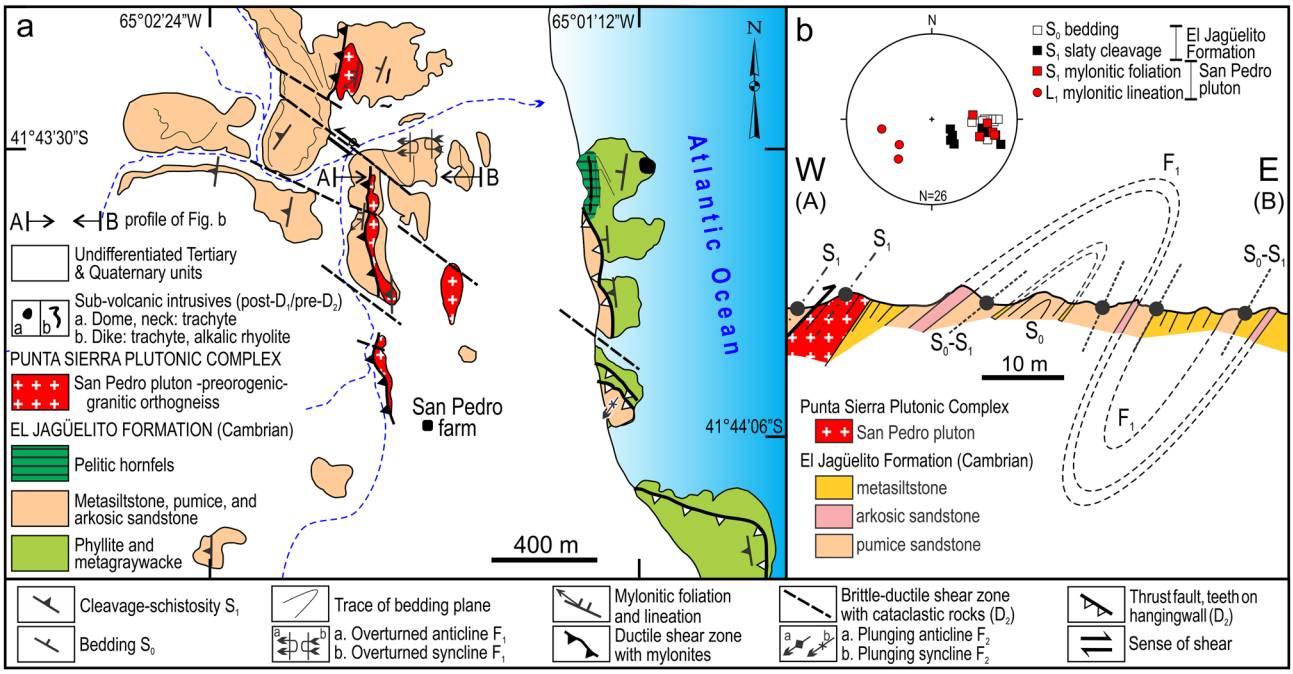

Fig. 10 **a** Geological map of the El Jagüelito Formation and the pre-orogenic San Pedro pluton in the south of the Punta Colorada area, based on field mapping. For the map location, see Fig. 3. **b** E–W trending geological profile exhibiting the D_1 structural features. See the profile location in (**a**). Stereoplots are lower hemisphere, equal-area projections of structural elements

Late-D_1 to pre-D_2 microstructures in shear zones

The S/C fabric of the phyllonites from west of the Hiparsa mine consists of a sigmoidal foliation S_1 oblique to discrete shear C planes (= mylonitic foliation). S_1 is defined by aligned quartz-feldspar aggregates and M_1 muscovite-biotite fishes indicating a sinistral sense of shear (Fig. 11g). C planes consist of chlorite-muscovite ± biotite aggregates overprinted partly by decussate micas.

The microfabrics of mylonites from the San Pedro pluton are typical to those derived from granitic protoliths, with feldspar-muscovite and quartz-biotite forming porphyroclasts and matrix, respectively. Feldspar porphyroclasts are stretched or fragmented into domino arrangements along with mica fishes. Quartzofeldspathic ribbons are parallel to the mylonitic foliation defined by muscovite-chlorite-biotite-fibrolite-epidote alignment (Fig. 11h). Elongate quartz sub-grains pass laterally into domains of fine-grained quartz formed by bulging. Retrogressed prismatic sillimanite defines the L_1 stretching lineation. Sillimanite-rich C'-type shear band cleavage transects the mylonitic foliation at low angles, confirming the sinistral sense of shear identified at the outcrop scale.

Kübler and Árkai indices

Results of the Kübler and Árkai indices summarized in Table 2 are presented in the correlation plots of Fig. 12. The values of the Kübler Index range between 0.16 and 0.33 Δ°2θ, mostly belong to the field of the epizone grade with a few meta-pelites within the upper anchizone-epizone transition. The Árkai Index range between 0.13 and 0.23 Δ°2θ, fitting entirely within the field of the epizone. Both indices agree well with the mineral assemblages described above.

EPMA data and chlorite thermometry

Electron microprobe analyses of chlorite and phengitic K-white mica were performed at the Electron Microprobe Laboratory (IGeo, U. São Paulo, Brazil), following standard procedures and analytical conditions summarized in the Online Resource 3. It also includes the analytical results and P–T constraints using geothermobarometers.

Temperature values obtained for pre-S_1 chlorite stacks range mostly between 298–320 °C (meta-siltstone SG07-7) and 328–363 °C (phyllite SG08-39-1). There are also two T-values of 268° and 299 °C for SG08-39-1. No temperature

Table 2 Summary of the low-grade metamorphic conditions M_1 obtained through multi-proxy approaches on the studied selected meta-pelitic samples from El Jagüelito Formation

Sample	Locality	Rock type	Petrography	DRX	Kübler Index Δ°2θ	Árkai Index Δ°2θ	Thermo-barometry	Observations
AS II-11-2-anticline-	lower Salado creek, east of Mussi farm	Phyllite	Ms-Bt-Chl-Qtz-Kf-Pl-Ap	Qtz-Ab-Chl-Ill-Kf-Pl-Sm	0.27	0.19		Chl-Zeol in axial planes F_2
AS II-12-2-syncline-		Slate	Qtz-Chl-Ill-Ab-Kf-Ms-Op	Qtz-Chl-Ill-Pl-Fel	0.19	0.17		Chl stacks
SG-07-7-syncline-		Meta-siltstone	Qtz-Ab-Ill-Chl	Qtz-Chl-Ill-Pl-Sm-Fel	0.20	0.23	298–320 °C 284–293 °C 3.06–3.16 kb	Chl stacks
AS II-14-syncline-		Meta-siltstone	Qtz-Chl-Ill-Ab	Qtz-Chl-Ill-Kf-Pl	0.21	0.16		Chl stacks
SG-12-16[a]-anticline-		Meta K bentonite	Qtz-Ill-Prh-Zeol-Ser	Qtz-Ill-Kf-Sm-Ser-Prh	0.33	–		Zeol porphyroblasts
AS-3[a]-anticline-	Herradura del Salado footwall	Meta-K bentonite	Qtz-Ser-Ill-Zeol-Chl-Prh	Qtz-Ill-Kf-Pl-Sm-Ser-kln	0.33	–		
SG-08-39-1-syncline-		Phyllite	Qtz-Chl-Ill-Ser-Ab	Qtz-Chl-Ill-Kf-Pl	0.22	0.19	328–363 °C	Chl stacks
SG-07-36-A-syncline-		Phyllite	Qtz-Chl-Ill-Ab	Qtz-Chl-Ill-Kf-Pl-Zeol-Mnt	0.26	0.16		Zeol veinlets parallel to S_1
SG-07-27-A-anticline-		Slate	Qtz-Ill-Ser-Ms-Chl-Stp	Qtz-Chl-Ill-Kf-Pl-Stp	0.31	0.19		
SG-07-29-syncline-		Phyllite	Qtz-Ill-Chl-Ms	Qtz-Chl-Ill-Kf-Pl	0.23	0.17		Chl-Ill stacks
SG-09-15	Herradura del Salado hanging-wall	Slate	Qtz-Chl-Ill-Ser	Qtz-Chl-Ill-Kf-Pl-Sm-Ser	0.24	0.21		
SG-09-16		Phyllite	Qtz-Chl-Ill-Pl	Qtz-Chl-Ill-Kf-Pl-Zeol-Ser	0.25	0.19		
SG-09-24-A	West of Hiparsa mine	Phyllite	Qtz-Chl-Ill-Kf-Pl	Qtz-Chl-Ill-Kf-Pl	0.16	0.13		
SG-09-24-B		Phyllite	Qtz-Chl-Ill-Ab-Kf	Qtz-Ab-Chl-Ill-Kf-Pl-Sm	0.17	0.22		

DRX: bulk mineralogy and composition of clay mineral fraction obtained with X-ray diffraction analysis. After the sample number, the associated F_1 folds are also indicated, when possible

[a]Recalculated after González et al. (2018). Mineral abbreviations after Kretz (1983), except: Sm: Smectite; Op: opaque minerals; Zeol: zeolites; Ser: sericite. Fel: feldspar *s.l.*, without mineral identification

differences are noticeable between the inner and outer parts of stacks (Fig. 1 of the Online Resource 3). Temperature values calculated for syn-S_1 chlorites range between 284 and 293 °C (SG07-7). They are lower than temperatures of pre-S_1 chlorite stacks of the same sample, and also of those of the phyllite SG08-39-1.

Pressure values found for a phengitic K-white mica range between 3.06–3.16 Kb for minimum and maximum-T of the syn-S_1 chlorites, which are in textural equilibria with the S_1 cleavage. The mean *b* unit cell dimension value of the same phengitic mica is 8.97 Å, indicating a low-pressure gradient for the S_1-formation event during M_1 metamorphism.

Discussion and interpretation

D_1-tectonic evolution

The structural evolution of the E-verging El Jagüelito fold-and-thrust belt is diachronous among the different basement outcrops of the Sierra Grande-Playas Doradas area, where each outcrop records a part of that evolution. The relative timing can be summarized as follows: (1) The onset of thrusting occurred roughly synchronous with syn-metamorphic folding, and fault-propagation folds seem to dominate in the external and lowest metamorphic part of

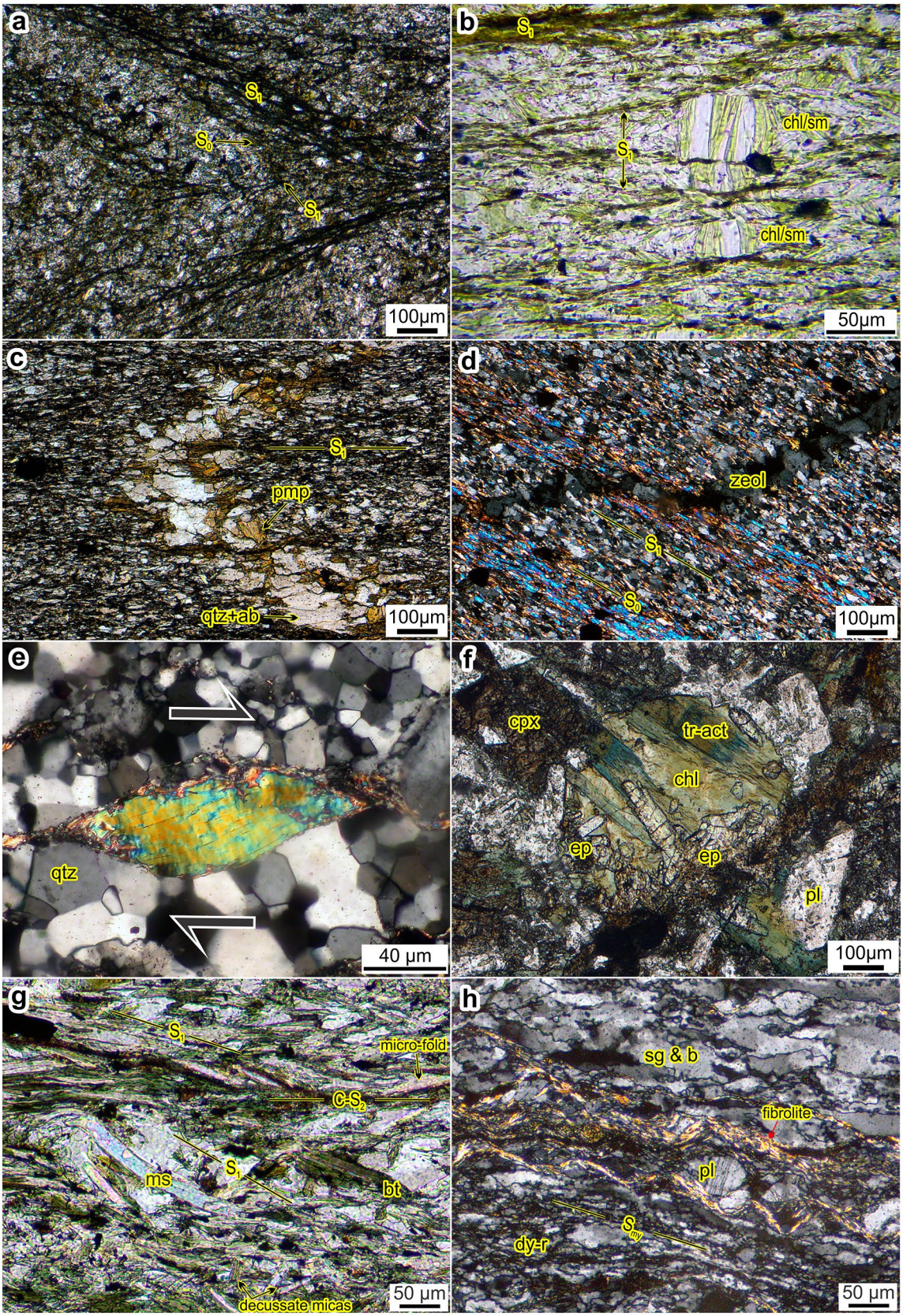
a
S1
S0
S1
100μm
b
S1
chl/sm
S1
chl/sm
50μm
c
S1
pmp
qtz+ab
100μm
d
zeol
S1
S0
100μm
e
qtz
40 μm
f
cpx
tr-act
chl
ep
ep
pl
100μm
g
S1
micro-fold
C=S2
S1
ms
bt
decussate micas
50 μm
h
sg & b
fibrolite
pl
Sm
dy-r
50 μm

◂**Fig. 11** Photomicrographs from thin sections, parallel or crossed polarizers, of the El Jagüelito Formation (**a**–**d**, and **g**) and Punta Sierra Plutonic Complex (**e**, **f**, and **h**). Mineral abbreviations are those of Kretz (1983). **a** Silty/argillaceous compositional bedding S_0 overprinted by micro-fold F_1 and S_1 slaty cleavage. Crossed polarizers. **b** Barrel-shaped, pre-S_1 illite-chlorite stacks in meta-pelite SG07-7. S_1 cleavage planes wrapped the porphyroblasts and strain caps/shadows. Parallel polarizers. **c** Quartz-albite-pumpellyite pre-S_1 veinlet cut the bedding S_0. They are, in turn, affected by a micro-fold F_1 and the associated axial plane cleavage S_1. Crossed polarizers. **d** Zeolite-pumpellyite post-S_1 veinlet intersecting the S_0–S_1 planes. Crossed polarizers. **e** Band of polygonal granoblastic aggregates of quartz parallel to S_1 foliation, accompanied by a muscovite fish indicating dextral shearing in a granitic mylonite of the pre-orogenic El Molino pluton. Parallel polarizers. **f** Amygdale filled with chlorite-epidote-tremolite/actinolite M_1 association in a meta-gabbro of the Herradura del Salado sill swarm. Plagioclase and clinopyroxene are relict igneous minerals. Parallel polarizers. **g** S/C fabric in a phyllonite from west of the Hiparsa mine area. Sigmoidal foliation S_1, displaced by discrete shear C planes (=mylonitic foliation), and muscovite-biotite fishes are indicating a sinistral sense of shear. Parallel polarizers. **h** Quartz ribbon parallels to mylonitic foliation (S_{my}) exhibiting dynamic recrystallization (dy-r) with sub-grains formed by bulging (sg-b) in a granitic mylonite of the pre-orogenic San Pedro pluton. Fribolitic sillimanite retrogressed partially to chlorite define the L_1 mylonitic lineation. Parallel polarizers

the belt (Fig. 4). The brittle-ductile deformation involving thrusting with a bed-parallel flexural slip is also supported by field observations of Giacosa and Paredes (2001). (2) Faulting outlasted folding but was completed before the D_2 shortening event (Figs. 6, 9, 10). It involves ductile or brittle-ductile shear zone deformation in deeper structural levels, also exhibiting higher metamorphic grades and stronger deformation effects, locally.

The kinematic history of faulting can likely be related to the eastward transfer of regional shortening above a basal *detachment* also affecting the much deeper crystalline basement rocks and may extend even into the lower crust. The geometry and kinematics of the folds and faults emphasize the essential control exerted by Patagonian lithosphere rheology, including D_1 structural and M_1 thermal inheritance, and local/regional boundary conditions on the different parts of the belt.

Stages of low-grade metamorphism M_1

Collectively, the regional metamorphism M_1 of the El Jagüelito Formation records three stages during the D_1-structural evolution of the fold-and-thrust belt. The stages evolved progressively from pre-kinematic (pre-D_1) zeolite facies through the main syn-kinematic (syn-D_1) prehnite-pumpellyite to greenschist facies, to final post-kinematic (post-D_1) prehnite-pumpellyite facies (Online Resource 1).

Pre-D_1 stage

Porphyroblasts affected by the S_1 cleavage point to a pre-kinematic heating, also indicated by veinlets emplacement due to fluids production/infiltration through devolatilization and hydro-fracturing, free of regional deformational features (e.g., Walther and Orville 1982; Jamtveit and Austrheim 2010). The pre-D_1 stage of M_1 took place at low temperatures between about zeolite-to-prehnite/pumpellyite facies and relatively low pressure, then resulting in a pattern of burial diastathermal metamorphism (e.g., Robinson 1987; Robinson and Bevins 1986). As temperature increases with depth, the regional heat flow before the onset of the El Jagüelito fold-and thrust belt deformation may have been high and was caused by several sources (see Sect. 7.1.1).

Syn-D_1 stage, Kübler-Árkai indices, and quantitative P–T constraints

The syn-kinematic main stage of the M_1 metamorphism coincides with the onset and progress of the fold-and-thrust belt deformation. The crystallization of the mineral assemblages was related to the formation of F_1 folds and related structures. Disparate metamorphic grade recorded among lithologies of the alternating syncline to an adjacent anticline F_1 along a fold-and-thrust belt section. Collectively, the mineral assemblages and Kübler-Árkai indices record the highest grade assemblages under greenschist facies conditions (chlorite-to-biotite grades) along the synclinal regions with psammo-pelitic rocks. Conversely, the lowest grade assemblages occur at the anticlinal portions containing volcanic rocks with prehnite-pumpellyite/pumpellyite-actinolite facies conditions (Figs. 4a, 8a; see also Fig. 1 of the Online Resource 2).

Disparate metamorphic grades within the same stratigraphic sequence can be reconciled as the folding of a pre-existing (pre-D_1) nearly horizontal burial isotherms (e.g., syn-metamorphic folding and faulting, Miyashiro 1994). The thermal relaxation in the course of quiescent periods of folding and faulting resulted in cooling in the anticlinal portions of the first F_1 folds and heating in the synclinal regions. The resulted syn-D_1 pattern is prograde orogenic metamorphism adjusting from P to T increases but did not go to equilibrate before metamorphism waned. The isotherm folding and re-equilibration was likely repeated along with the fold-and-thrust belt evolution, resulting in intricate isograd patterns and mineral reaction histories (e.g., Page Chamberlain 1986; Miyashiro 1994).

Al^{IV}-in-chlorite thermometry and Si-in-phengite barometry indicate P–T conditions of the lower part of greenschist facies transitional with prehnite-pumpellyite facies, following the mineral assemblages and Kübler-Árkai indices (Table 2, Online Resource 3). T-values for the syn-S_1 stage

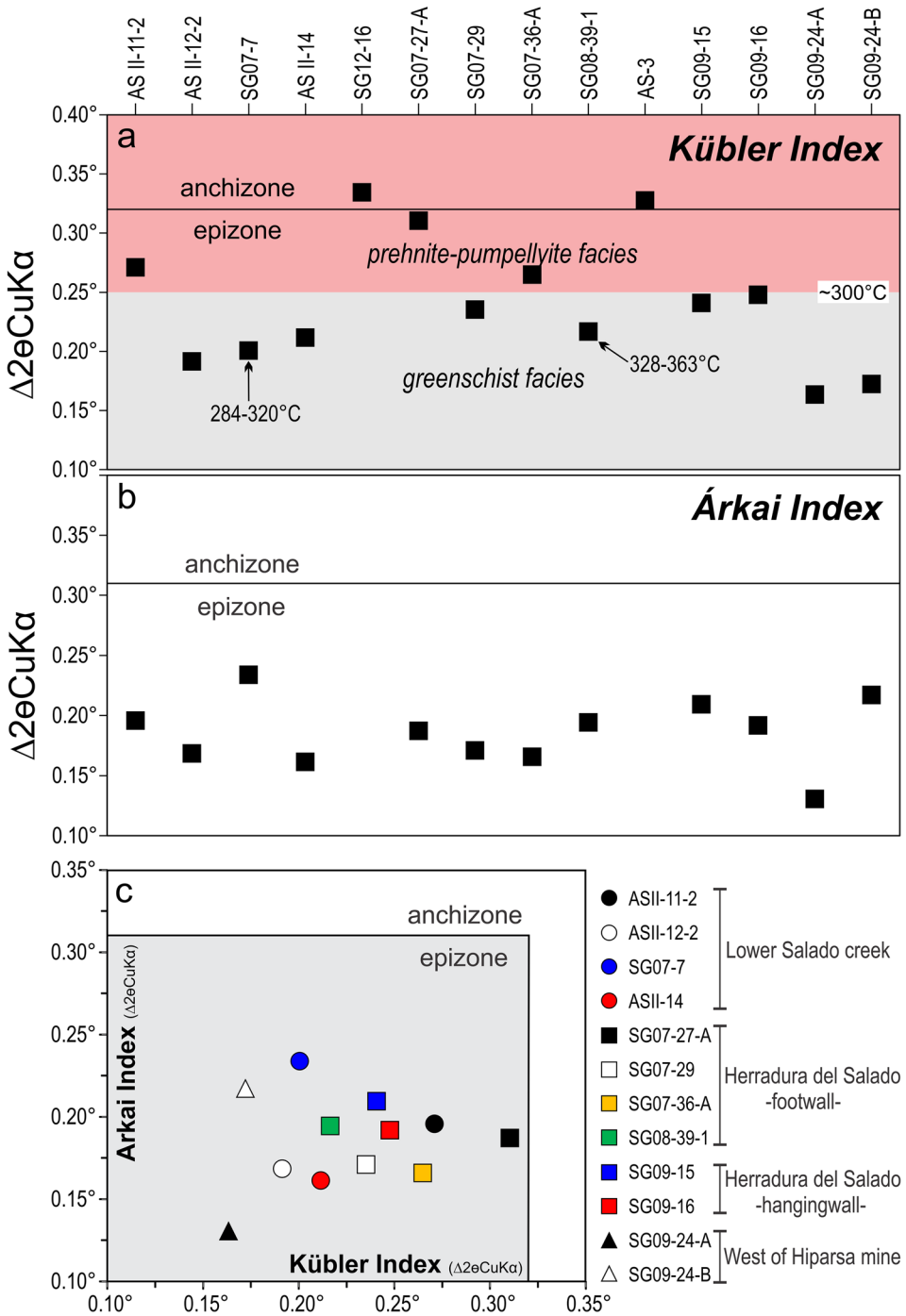

Fig. 12 **a**, **b** Correlation plots of illite (Kübler) and chlorite (Árkai) crystallinity indices with metamorphic zones and facies for the studied pelitic samples. The lower and upper anchizone boundary values are based on Kübler Index values of 0.52° and 0.32° Δ°2θ, respectively, which are the Frey-Kübler equivalent for the CIS scale of measurement (Kübler et al. 1979; Warr and Ferreiro Mahlmann 2015, Merriman and Peacor 1999). The Kübler equivalent upper and lower boundaries of the CIS anchizone at 0.32 and 0.52 Δ°2θ can be translated to Árkai Index values of 0.31° and 0.41°2θ, respectively (Warr and Cox 2016; Árkai et al. 1995, see also Árkai 1983, 1991)

are lower than those of the pre-S_1 stage, and the pressure obtained is related to S_1 cleavage formation through syn-D_1 (see data in Sect. 5.5). Then, peak-T and peak-P conditions are diachronic and reached in pre-D_1 and syn-D_1 times, respectively, i.e., before and in the course of the axial plane cleavage S_1 formation. Shortening reached at a maximum during the cleavage formation, also in coincidence with the climax of the fold-and-thrust belt development. This led the interpretation that the relatively low-P condition of the syn-D_1 stage was higher than that of the pre-D_1 stage. Accordingly, a low-P gradient for the syn-D_1-M_1 stage points toward a low-pressure facies series with inferred geothermal gradient > 35 °C km^{-1} (*b* values lower than 9.000 Å are typical of low-P, Guidotti and Sassi 1986).

Post-D_1 stage

After peak P–T was reached, overall decreasing temperature and pressure led to the formation of post-tectonic porphyroblasts and veinlets, overprinting and intersecting the S_1 cleavage planes, respectively (Fig. 7d, Online Resource 1). After cessation of D_1 shortening, a new phase of fluids production/infiltration by hydro-fracturing occurred resulting in a pattern of retrogressive metamorphism. Simultaneous cooling and decompression took place under the transition between zeolite and prehnite-pumpellyite facies, also involving thermal relaxation and re-hydration of basement slices.

P–T–D-time path

Integrating the three thermal stages resulted in a mono-phase trajectory describing an *anti-clockwise P–T–D-time* evolutionary path for the D_1-M_1 event (Fig. 13). The pre-kinematic segment of relict prograde metamorphism involved burial until reaching peak-T, and followed by a syn-kinematic loop in which rocks achieve peak-P conditions. Then, a post-kinematic retrograde counterpart is related to decreasing P–T conditions. Geodynamic implications of each part can be ascribed as low-P burial heating during the overall deposition of the volcano-sedimentary pile, followed by basin inversion and higher-P overprint due to shortening and tectonic loading, and final post-orogenic collapse with exhumation. Such a type of P–T trajectory characterizes low-grade metamorphic terranes in extension-contraction tectonic settings (Merriman and Frei 1999).

Low-grade metamorphism M_1 of the pre-orogenic igneous suite

In the pre-orogenic plutons of the Punta Sierra Complex, the syn-D_1 to post-D_1 stages display widespread mineral assemblages typical of the transition between prehnite-pumpellyite and greenschist facies, correlating to those of the intercalated rocks of the El Jagüelito Formation (Online Resource 1). Syn-D_1 microstructures in the El Molino pluton revealed greenschist facies conditions under biotite grade, probably < 400 °C (e.g., Stipp et al. 2002). Yet, syn-D_1 disequilibrium mineral assemblages in the Herradura del Salado mafic rocks are indicative of the transition from prehnite-pumpellyite to either greenschist or prehnite-actinolite facies, and even tremolite-actinolite plus pumpellyite facies (e.g., Hashimoto 1966; Banno 1998). They suggest a T-range of 290–330 °C at relatively low-P (e.g., Willner et al. 2009; Starr et al. 2019). A post-D_1 set of veins intersecting S_1 cleavage planes exhibits retrograde mineral assemblages representing the passage from prehnite-actinolite to prehnite-pumpellyite facies.

Late-D_1/pre-D_2 high-grade, local shear zone metamorphism

Deeper structural levels involved in late sheets of the fold-and-thrust belt alternate medium greenschist to amphibolite facies dynamic metamorphism (Figs. 6, 10). Late-D_1/pre-D_2 local high-grade metamorphism related to shear zone deformation overprints the regional D_1–M_1 pattern. The localized thermal up-grade is likely associated with tectonic loading following the emplacement of earlier thrust slices.

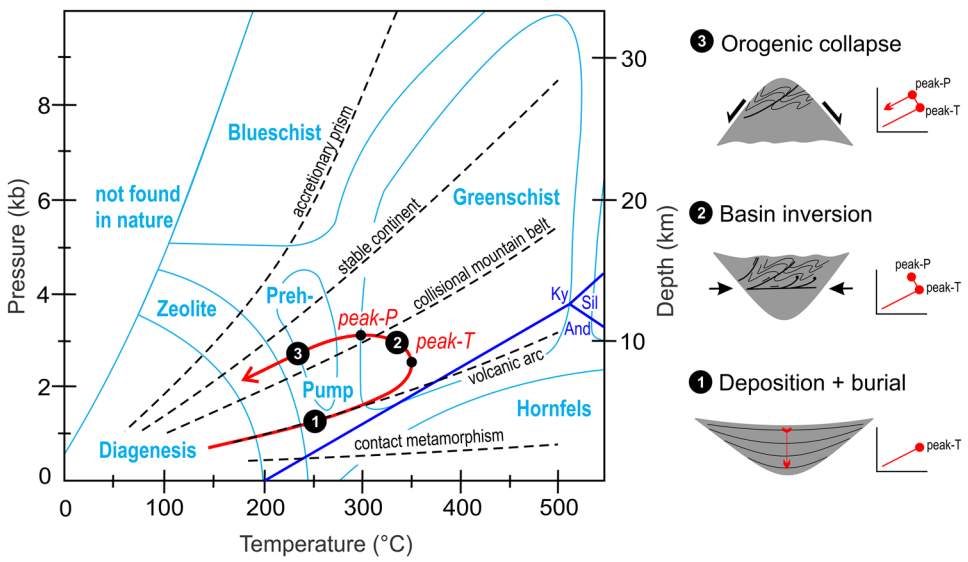

Fig. 13 Schematic anti-clockwise P–T-time metamorphic path for the studied meta-pelites SG07-7 and SG08-39-1. P–T data as in Online Resources 2 and 3. The right side of the figure depicts the geodynamic implications for each segment. See details of the evolution in the text

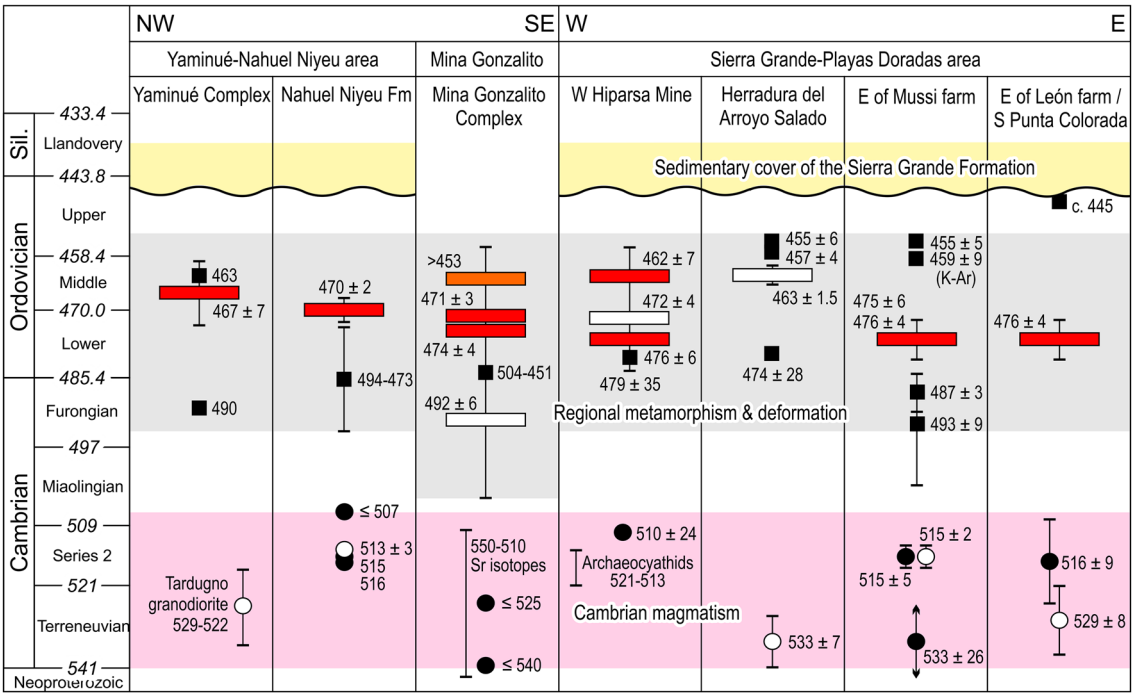

Fig. 14 Schematic tectonometamorphic sections (modified from González et al. 2018) of the basement units correlated along NW–SE cross-section of the eastern North Patagonian Massif. For the profile location, see Fig. 2. U–Pb data (ages in Ma): black square: rims or Pb loss in detrital/magmatic zircons; black circle: detrital zircons in meta-sedimentary protoliths; white circle: magmatic zircons in meta-igneous protoliths. References to U–Pb zircon data: Pankhurst et al. (2006); Rapalini et al. (2013); Greco et al. (2014, 2015, 2017); González et al. (2008a, 2018) and Varela et al. (1998, 2008, 2011b, 2014). Age of the sedimentary cover based on Rustan et al. (2013) and Sicardi et al. (2014). The ICS International Chronostratigraphic Chart of Cohen et al. (2013, updated) has been used

Timing of metamorphism M_1, deformation D_1, and magmatic activity

Combining the tectonometamorphic results presented in this contribution, the available geological and U–Pb zircon data of the El Jagüelito Formation and Punta Sierra Plutonic Complex allow assessing the D_1–M_1 timing of the El Jagüelito fold-and-thrust belt (Fig. 14). After Fortunian-Stage 4 (Cambrian) deposition of the volcano-sedimentary pile of the El Jagüelito Formation, the pre-D_1–M_1 stage could have likely been developed between the Furongian and Tremadocian (493–474 Ma). Subsequently, the syn-D_1–M_1 stage, along with the emplacement of pre- and post-orogenic intrusive suites of the Punta Sierra Complex, occurred during the Floian-Darriwilian interval (476–462 Ma). The overall basement exhumation can be constrained, at least, to the Sandbian-Katian time, as is also supported by the Upper Ordovician (Hirnantian) maximum depositional age of the Sierra Grande Formation, which unconformably overlies the basement.

As can be seen from the above, the tectono-magmatic igneous-metamorphic basement evolution was episodic and distributed in overlapping pre-, syn-, and post-orogenic stages, which was active at different crustal levels. Shallow emplacement of the pre-orogenic igneous bodies into undeformed protoliths is roughly coeval with the intrusion of the post-orogenic plutons into the already deformed and superficially exhumed belt. Then, the syn-D_1–M_1 stage took place diachronous for the same unit but from different structural levels, a little older at deeper higher-grade rocks than in those of the shallow lower grade (e.g., Lardeaux 2014). In higher structural levels, spatial and temporal overlapping of the post-D_1–M_1 stage and post-orogenic intrusions could also be likely.

Accordingly, the timing of the tectonometamorphic D_1–M_1 event and associated magmatic activity, related to a discrete and short-lived orogeny, is constrained to the late Cambrian-Middle Ordovician, with an evolutionary history of ~ 30 Ma that characterizes accretionary orogenic belts (Collins 2002; Cawood et al. 2009; Brown 2010).

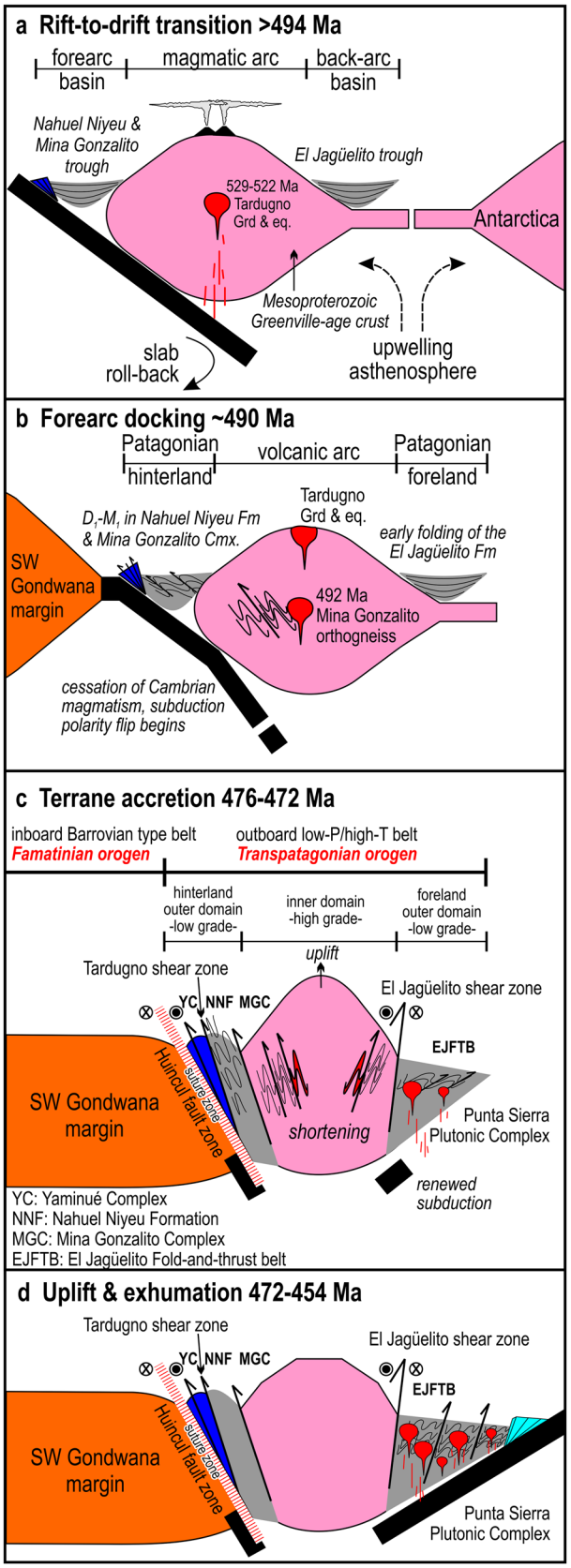

Fig. 15 **a–d** Geodynamic evolutionary stages of the tectonometamorphic units belonging to northern Patagonia terrane through the early Paleozoic (schematic sketches). For explanations, see text ▶

Geodynamic implications

Tectonic stages

Considering a magmatic arc-back arc terrane as the most likely geotectonic setting (González et al. 2018), a series of tectonic evolutionary stages with geodynamic implications can be derived to the early Paleozoic basement of the North Patagonian Massif (Fig. 15),

Rift-to-drift transition

Pre-D_1–M_1 high heat flow and steep geothermal gradients are compatible with a thinned and thermo-rheologically weakened crust in an extensional back-arc region (e.g., Miyashiro 1967,1973; Schulmann et al. 2002). A magmatically underplated arc crust involved an external heat source from the mantle upwelling during Cambrian rifting (González et al. 2018). Basin subsidence driven by a thermo-tectonically unstable back-arc region supported the rapid expansion of the accommodation space and sediment supply for increasing burial with diastathermal metamorphism (e.g., Robinson 1987; Robinson and Bevins 1986). Then, the most likely geodynamic scenario is a rift-to-drift transition that marks the phase in which a retreating back-arc gives way to detaching northern Patagonia terrane from East Antarctica (Fig. 15a).

Terrane accretion

Terrane docking and final amalgamation against the southwestern continental margin of Gondwana triggered switching from extensional to compressional settings. Progressive deformation and metamorphism are diachronous (Fig. 14), starting earlier in the forearc basin of the Nahuel Niyeu Formation due to the first arrival, and reaching the back-arc later (Fig. 15b, c). As a result of the active compressional mountain-building phase, an accretionary orogen developed outboard of the margin, inboard of which lies the early Paleozoic Famatinian collisional orogen. The mode of coupling along convergent plate boundaries that drove orogenesis led to the development of a NW–SE trending *paired metamorphic belt system*, with two parallel linear belts of basement rocks with contrasting metamorphic patterns separated by a suture zone.

Uplift and crustal thickening during the orogeny suggest a tectonic loading by a ~ 12 km-thick crustal pile (2.8 g/cm^{-3} as mean crustal density and the inferred geothermal gradient > 35 °C km^{-1}), compatible with low-P

facies metamorphic series (e.g., Guidotti and Sassi 1986). Then, the overprinting syn-D_1–M_1 event is suitable with an accretion assembly of a magmatic arc, following an anticlockwise P–T–D-time path (e.g., Yamamoto 1993; Wakabayashi 2004; Cawood et al. 2009; Willner et al. 2014).

The orogenic events in deep-to-shallow crustal levels correspond with the angular unconformity between the basal layers of the Sierra Grande Formation and the early basement slices of the El Jagüelito Formation at the surface. The syn-orogenic clastic accumulation of a basal conglomerate containing metamorphic clasts of the underlying basement is the sedimentary response to uplift by compressive mountain building (Naipauer et al. 2011).

Uplift and exhumation

After the end of mountain building, overall cooling and decompression of the basement slices by thermo-tectonic relaxation can likely be the result of an oceanward extensional collapse of the colliding terrane. Although clear structural evidence for such collapse is likely overprinted by Permian Gondwanide shortening, the emplacement of post-orogenic magmas, on the one hand, is a signal for post-collisional extension (Fig. 15d, González et al. 2020). A transition from subduction roll-back to subduction polarity reversal seems to be a relaxation phase favorable for the ascent of magmas generated during the period of maximum convergence (i.e., the collision *s.str.*) in post-collisional settings (Liégeois 1998).

On the other hand, denudation of the Ordovician orogen by erosion and southward spread out of basement slices occurred through western North Patagonian Massif to North Patagonian Cordillera, resulting in the post-orogenic sedimentary record of Siluro-Devonian protoliths. U–Pb detrital zircon age spectra with 480–460 Ma as one of the main provenance patterns (Hervé et al. 2018; Uriz et al. 2019) indicate that the orogen was an emerged source area. Yet, the hiatus of around 40 My existing within the Sierra Grande Formation emphasize the syn-orogenic and post-orogenic character of the basal conglomerate (Naipauer et al. 2011) and the youngest members (Uriz et al. 2011), respectively.

The Ordovician Transpatagonian orogenic belt

Definition and boundaries

The early Paleozoic orogenic cycle of regional distribution in northern Patagonia formed a mountain range that shall be named the *Transpatagonian Orogen* (TPO), and the *Transpatagonian Orogeny* refers to the tectonometamorphic and magmatic activity. As part of a paired metamorphic belt system, the TPO is the outboard low-P/high-T belt, and the parallel, inboard medium-P/T belt of Barrowian type, is the Famatinian orogen on the autochthonous Gondwana margin.

The TPO has a general NW–SE trending orogenic axis across northern Patagonia. The orogen is ~ 500 km long and 200–400 km wide. The belt consists of long arcuate strips of crystalline igneous-metamorphic basement rocks that extend, interrupted by outcrops of the Cenozoic basaltic Somuncura plateau, from the pre-Andean foothills in the west to coast of the Atlantic Ocean (Playas Doradas) in the east. The orogen can likely be as long as ~ 1000 km, considering southeastward continuation within the Argentine continental shelf (Fig. 16).

Along 39°–40°S, the TPO is juxtaposed tectonically against the basement of the Famatinian orogen in the north, alongside the E–W oriented Huincul Fault Zone, which is a continental-scale structural lineament extending from the Chilean Coast Range eastwards into the Argentine continental shelf (e.g., Turner and Baldis 1978; Ramos et al. 2011). As a long-lived geological and geophysical discontinuity, it was proposed to represent the suture zone between Patagonia and the Gondwana margin (Ramos 1984; Ramos et al. 1986, 2004).

On the southern side, the TPO encompasses the NW–SE trending continental-scale geological and

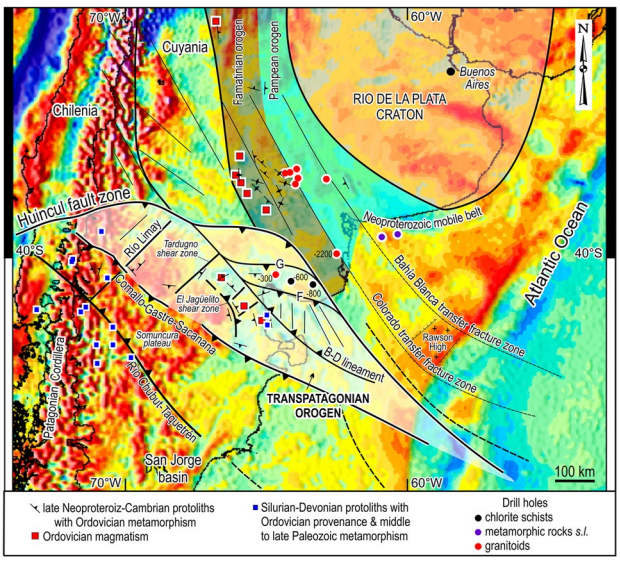

Fig. 16 Location of the Transpatagonian orogen concerning the South American terranes west of the Río de la Plata craton, the major terrane boundaries, and the Pampean and Famatinian orogenic belts. The Huincul Fault Zone showed as in Ramos et al. (2004), whereas the Comallo-Gastre-Sacanana and Rio Chubut-Taquetrén lineaments as in Renda et al. (2019). The base map is a color image of the free-air gravity field model downloaded from the International Centre for Global Earth Models (Barthelmes and Köhler 2016; Ince et al. 2019; web site: https://icgem.gfz-potsdam.de/home). The final depths of the drill holes in the map refer to the lithologies shown. See details in the text

geophysical discontinuity of the Comallo-Gastre-Sacanana lineament (Gregori et al. 2013; Renda et al. 2019). It extends from the North Patagonian Cordillera in the west to the coast of the Atlantic Ocean into the continental shelf. The lineament likely separates the southernmost early Paleozoic basement slices of the North Patagonian Massif from either the pre-Devonian high-grade Cáceres Igneous-Metamorphic Complex (Giacosa et al. 2014) or the subsurface Paleozoic basement of the San Jorge basin in the south (Fig. 1).

The eastern side can be traced from the outcrops in Playas Doradas eastward into the Argentine continental shelf through the southeastern convergence area of the Comallo-Gastre-Sacanana lineament/Huincul Fault Zone. Both faults are parallel to the Colorado and Bahía Blanca transfers (Fig. 16; Franke et al. 2007), which are fracture zones oblique to the continental margin separating basement blocks belonging to Gondwana and Patagonia (e.g., "the Permian granitic province" or the "Rawson high"; Ewing et al. 1963; Fryklund et al. 1996; COPLA 2017).

On its western side, the Río Limay lineament marks the boundary of the TPO, which is likely juxtaposed (tectonically?) against the Devonian to Permian igneous-metamorphic basement belonging to the Cordillera Neuquina-Neuquén Basin to the west (e.g., Piedra Santa and Cuesta de Rahue basements, Cingolani et al. 2011).

Tectonometamorphic domains

Based on the structural geometry and metamorphic grade, the TPO can be internally divided into four domains. From NW to SE, the orogen is double-sided, consisting of two outer domains with low-grade rocks of the Nahuel Niyeu (hinterland) and El Jagüelito formations (foreland), embracing an inner domain or axial zone with high-grade rocks of the Mina Gonzalito Complex. The high-grade Yaminué Complex could represent dismembered parts of an accretionary prism domain, given its disparity of protoliths, tectono-magmatic ages, and structural complexity, sandwiched between the hinterland and the basement of Famatinian orogen on the Gondwana margin. The Punta Sierra Plutonic Complex represents the arc magmatism, which are more voluminous in the axial zone (Fig. 2a, b).

The domains are bounded tectonically by an orthogonal set of NW–SE and NE–SW-trending faults/structural lineaments. These are parallel and transversal to the suture Huincul Fault Zone and Comallo-Gastre-Sacanana lineament, limiting the orogen towards north and south, respectively (Fig. 17a). The NW–SE trending mylonitic belt of the El Jagüelito ductile shear zone juxtaposed the Mina Gonzalito domain toward SW over the El Jagüelito domain, which likely occurred during terrane accretion. It also indicates oceanward extrusion of the colliding basement slices northward. SE- and E-directed migration of the orogenic front in the Nahuel Niyeu and El Jagüelito domains, respectively, can be the result of the orogen-parallel terrane juxtaposition along the Huincul Fault Zone, combined with internal decoupling of the low- and high-grade domains along NE–SW-trending faults. Likewise, in the hinterland, the NE–SW trending Tardugno shear zone juxtaposed the Tardugno Granodiorite-Yaminue Complex pair against the Nahuel Niyeu Formation along S to SW-directed thrusting and accompanied progressive deformation (Chernicoff and Caminos 1996b; von Gosen 2003; Greco et al. 2015).

Prolongation of the TPO along the orogenic axis

The main tectonometamorphic domains delineate the core architecture of emerged parts of the TPO in the eastern North Patagonian Massif. Remnants of low-to-high-grade metamorphic rocks bounded by the Comallo-Gastre-Sacanana lineament and Huincul Fault Zone convergence zones can likely be extensions of the orogen towards NW and SE. The foreland El Jagüelito domain could continue southeastward along the E–W trending belt of phyllites, schists, and pelitic hornfels of the El Refugio and La Irene areas (Haller 1981; Cortés 1987). The foliation planes in the simple deformed rocks are S-dipping, suggesting a N-directed tectonic transport of the basement slices (Fig. 17a). This part of the orogen could extend offshore into the continental shelf.

In western North Patagonian massif, the NW–SE trending and NE-dipping strips of schist, gneisses, and migmatites (Núñez and Cucchi 1990; González and Cucchi 1994) of the Blancura-Mencué area correlate to those of the axial Mina Gonzalito domain, though geochronological constraints are needed to support this interpretation. The discontinuous NW–SE to E–W-trending and S-dipping strip of phyllites between the Colo Niyeu and Quili Malal areas can be considered as the correlative equivalent of the Nahuel Niyeu domain, owing to its low-grade metamorphism and outward hinterland position to the north, concerning the high-grade Blancura-Mencué rocks in the south (Fig. 17a). Despite a poor outcrop situation and heterogeneous degree of structural information, U–Pb zircon age constraints indicate Cambrian deposition and an Ordovician tectonometamorphic event (c. 475 Ma, Martínez Dopico et al. 2017) to Colo Niyeu meta-sedimentary sequence. According to the southward-dipping fabric, we assume a N- to NE-directed tectonic transport of the phyllitic slice.

The TPO in the subsurface of the Colorado basin

Available surface and subsurface geological-geophysical data of the Colorado basin led to the interpretation that, at least, three NW–SE trending and northward-imbricated basement sheets are involved in the TPO. They are

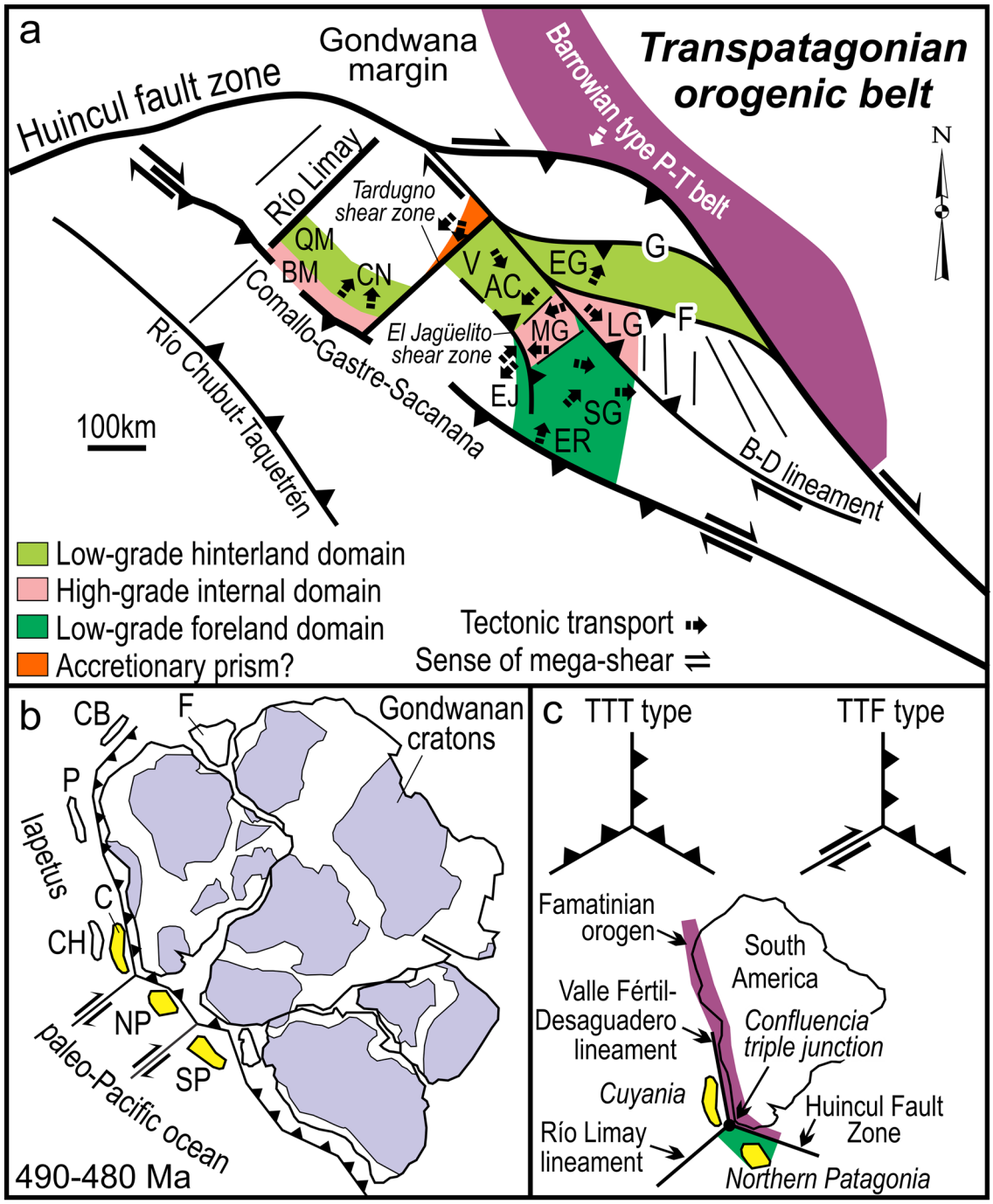

Fig. 17 **a** Schematic map showing the plate tectonic setting for the northern Patagonia terrane with the related outboard Transpatagonian orogen by Lower Ordovician. Dextral oblique subduction of the Patagonian plate deduced from the tectonic framework of the study area, combined with the regional available data throughout the different basement domains (Table 1). Localities: *BM* Blancura-Mencue, *QM* Quili-Malal, *CN* Colo-Niyeu, *NN* Nahuel Niyeu, *V* Valcheta, *AC* Aguada Cecilio, *MG* Mina Gonzalito, *EG* Bajo del Gualicho, *LG* Las Grutas, *SG* Sierra Grande, *ER* El Refugio-La Irene. **b** Gondwana configuration at 490–480 Ma time interval exhibiting the outboard situation of Gondwanan parautochthonous and Laurentian allochthonous terranes, reassembled along the (paleo-) Pacific-Iapetus margin of Gondwana by early Paleozoic. The Cuyania (C), Northern Patagonia (NP), and Southern Patagonia (SP) terranes are separated by two major dextral faults. Other terranes: *F* Florida, *CB* Chibcha, *P* Paracas, *CH* Chilenia. Figure modified from González et al. (2018) and Schmitt et al. (2018), and references therein. c Geometric framework between the three independent plates containing the Northern Patagonia and Cuyania terranes and the continental margin of Gondwana South America. They are separated by a triple junction (based on McKenzie and Morgan 1969) likely located around the "Confluencia triple-point" area (actual coordinates) in northern Patagonia

sandwiched between the suture Huincul Fault Zone and the so-called *"B–D" lineament* (Gregori et al. 2008, 2013), which is an internal geophysical discontinuity of the orogen oriented at an angle to the suture zone.

In the Salinas del Gualicho, the stratigraphic and tectonometamophic features of a phyllitic/granitic sheet intercalated between *"G"–"F" lineaments* (Gregori et al. 2008, 2013) correlate to those of the Nahuel Niyeu and El Jaguelito domains, though its position in the hinterland against the Gondwana margin (Figs. 16, 17a). Given the NW–SE to E–W trending and S–SW-dipping cleavage planes of phyllites and schists, it is reasonable to assume a N- to NE-directed tectonic transport of the metamorphic succession.

The study of Kaasschieter (1965) shows two drill holes inland of the Colorado basin recording chlorite schists that might be part of the northern margin of the North Patagonian Massif (Fig. 16). Their drill data also show that a granitic basement exists towards east, also corroborated by gravimetric, magnetometric, and seismic data (Kostadinoff 1992), but without age constraints yet. Accordingly, a continuous belt with low-grade rocks/granitoids can be traced parallel to the "G" and "F" lineaments from Salinas del Gualicho toward the east in the subsurface of the Colorado basin into the offshore areas.

A NW–SE trending wedge-shaped sheet composed of the high-grade Las Grutas Igneous-Metamorphic Complex is tectonically imbricated between "F" and "B–D" lineaments, and bounded by low-grade domains to the north and south. Lithologies and polyphase tectonometamorphic and magmatic evolution allow considering the complex as the correlative equivalent of the axial Mina Gonzalito domain, although only a few radiometric data are available (Sato et al. 2004). SE-directed thrusting of the complex (González et al. 2008c) can likely indicate tectonic escape with extrusion of the high-grade sheet from the embracing low-grade domains (Fig. 17a).

Plate tectonic setting of the TPO

Given the emerged and subsurface lithospheric framework of the TPO, Patagonia may have been part of an ancient independent micro-plate, as was previously inferred by von Gosen (2003). A triple junction of either TTT- or TTF-type (e.g., McKenzie and Morgan 1969) separated Patagonian from two other plates, i.e., the (paleo-) South American continent and Cuyania terrane. The crustal Valle Fértil-Desaguadero, Río Limay, and Huincul lineaments likely represent the major terrane boundaries separating the three paleo-plates. They join in the "*Confluencia triple junction*" (Fig. 17b, c).

An oblique subduction of the Patagonian plate is envisaged as a likely kinematic model for the accretion of the Northern Patagonia terrane. The oblique-slip vector would be partitioned into dip-slip orthogonal and lateral components, responsible for pure thrusting in the subduction zone and strike-slip faulting parallel to the margin, respectively. Diachronic coupling of the domains moving from SE to NW indicates convergent boundaries displaying dextral oblique plate motion.

Dextral margin-parallel translation of crustal blocks outboard of the continental margin has also already been proposed as a major tectonic feature of the late Paleozoic Gondwanide orogeny (Gregori et al. 2008). Owing to the TPO has been dissected and split into different crustal fragments during Gondwanide deformation, would imply that many faults/lineaments shown in Figs. 16 and 17 are either reactivated older faults or younger Gondwanide faults (Giacosa 2020). In addition, the varying tectonic transport directions in the different tectonic domains might argue for such an interpretation.

Conclusions

Studies in the eastern North Patagonian Massif permit the distinction of successive stages of tectonometamorphic events and intrusive activity as follows:

1 A Lower-Middle Ordovician orogenesis affected the Sierra Grande-Playas Doradas area. It included one event of ductile deformation D_1 accompanied by low-grade metamorphism M_1 and two successive plutonic pulses recorded as pre-orogenic and post-orogenic intrusions concerning the D_1–M_1 event.
2 The most striking tectonometamorphic D_1-M_1 feature is the El Jagüelito fold-and-thrust belt with an anti-clockwise P–T–D-time evolutionary path. Pre-D_1 prograde metamorphism involved peak-T; syn-D_1 achieves peak-P conditions, and post-D_1 is related to retrogression.
3 The Transpatagonian Orogeny built the Transpatagonian accretionary Orogen related to accretion of the northern Patagonia terrane against the (paleo-) Pacific-Iapetus continental margin of Gondwana.
4 The Transpatagonian Orogeny was short-lived and spatially limited to the accretion zone, with a migrating front from SE to NW in harmony with the obliquely subducted plate.
5 The early Paleozoic geotectonic framework for the contemporaneous occurrence of the contrasting Famatinian and Transpatagonian orogens along the southwestern Gondwana margin cannot be reconciled as the southern continuity of the first orogen in the second, but as a record of the orogen-parallel terrane juxtaposition by NW–SE accretion of contemporary belts of contrasting types.

6 A paired metamorphic belt system is recognized, with an outboard low-P/high-T belt (northern Patagonia terrane) and a parallel, inboard medium-P/T belt of Barrowian type (Gondwana margin). They are juxtaposed tectonically by dextral strike-slip motion along the Huincul Fault Zone.

7 The NW–SE trending structural framework of the Transpatagonian Orogen, with transversal offsets, is the oldest and most striking feature of northern Patagonia. It controlled reworking of crustal slices during the Gondwanide orogeny and younger times.

Acknowledgements We want to express our sincere thanks to people from the Sierra Grande area, all over the full eastern part of the Río Negro province, for allowing us access to their farms and for their hospitality during our fieldwork. We also thank G. Greco, H. Campos, V. García, and S. González for helping field mapping. The authors thank S. Oriolo and R. Suárez for valuable feedback on an early draft of this manuscript. We warmly acknowledge the reviews by V. A. Ramos and W. von Gosen, which improved the original manuscript significantly. This work was funded by Universidad Nacional de Río Negro (PI-UNRN-40-A-462 and PI-UNRN-40-A-622) and the Ministerio de Ciencia, Tecnología e Innovación Productiva, Agencia Nacional de Promoción Científica y Tecnológica (FONCYT, PICT-2015-0787).

References

Aceñolaza F, Toselli A (1976) Consideraciones estratigráficas y tectónicas sobre el Paleozoico Inferior del Noroeste Argentino. Proc II Congreso Latinoamericano de Geología 2:233–256

Árkai P (1983) Very low- and low-grade Alpine regional metamorphism of the Paleozoic and Mesozoic formations of the Bükkium, NE Hungary. Acta Geol Hungarica 26:83–101

Arkai P, Sassi F, Sassi R (1995) Simultaneous measurements of chlorite and illite crystallinity: a more reliable geothermometric tool for monitoring low- to very low-grade metamorphisms in metapelites. A case study from the Southern Alps (NE Italy). Eur J Mineral 7:1115–1128

Banno S (1998) Pumpellyite-actinolite facies of the Sanbagawa metamorphism. J Metamorph Geol 16:117–128

Barthelmes F, Köhler W (2016) International Centre for Global Earth Models (ICGEM). In: Drewes H, Kuglitsch F, Adám J. et al. The Geodesist's Handbook 2016. J Geod 90:907–1205

Basei M, Varela R, Sato A et al (2002) Geocronología sobre rocas del Complejo Yaminué, Macizo Norpatagónico, Río Negro, Argentina. Proc XV Cong Geol Arg 3:117–122

Brown M (2010) Paired metamorphic belts revisited. Gond Res 18:46–59

Busteros A, Giacosa R, Lema H (1998) Hoja Geológica 4166-IV, Sierra Grande (Río Negro). IGRM-SEGEMAR Boletín 241:1–75

Caminos R, Llambías E (1984) El Basamento Cristalino. In: Ramos V (ed) Geología y Recursos Naturales de la Provincia de Río Negro. Relatorio IX Cong Geol Arg 1(2):37–63

Caminos R, Chernicoff J, Fauqué L, Franchi M (2001) Hoja Geológica 4166-I, Valcheta, provincia de Río Negro. IGRM-SEGEMAR Boletín 310:1–73

Casquet C, Dahlquist J, Verdecchia S et al (2018) Review of the Cambrian Pampean orogeny of Argentina; a displaced orogen formerly attached to the Saldania Belt of South Africa? Earth-Sci Rev 177:209–225

Cathelineau M (1988) Cation site occupancy in chlorites and illites as function of temperature. Clay Miner 23:471–485

Cawood P (2005) Terra Australis Orogen: Rodinia breakup and development of the Pacific and Iapetus margins of Gondwana during the Neoproterozoic and Paleozoic. Earth-Sci Rev 69:249–279

Cawood P, Buchan C (2007) Erratum to "Linking accretionary orogenesis with supercontinent assembly" by P.A. Cawood and C. Buchan (Earth-Science Reviews 82 (2007) 217–256). Earth-Sci Rev 85(1–2):82–83

Cawood P, Kröner A, Collins W et al (2009) Accretionary orogens through Earth history. Geol Soc London Sp Pub 318:1–36

Chernicoff J, Caminos R (1996a) Estructura y relaciones estratigráficas de la Formación Nahuel Niyeu, Macizo Nordpatagónico oriental, provincia de Río Negro. Rev Asoc Geol Arg 51(3):201–212

Chernicoff J, Caminos R (1996b) Estructura y metamorfismo del Complejo Yaminué, Macizo Nordpatagónico, Provincia de Río Negro. Rev Asoc Geol Arg 51(2):107–118

Chernicoff J, Zappettini E (2004) Geophysical evidence for terrane boundaries in South-Central Argentina. Gond Res 7(4):1105–1116

Chernicoff J, Zappettini E, Santos J et al (2010) The southern segment of the Famatinian magmatic arc, La Pampa Province, Argentina. Gond Res 17:662–675

Chernicoff J, Zappettini E, Santos J et al (2013) Combined U-Pb SHRIMP and Hf isotope study of the Late Paleozoic Yaminue Complex, Río Negro Province, Argentina: implications for the origin and evolution of the Patagonia composite terrane. Geos Front 4:37–56

Cingolani C, Zanettini J, Leanza H (2011) El basamento ígneo y metamórfico. Geología y Recursos Naturales de la Provincia de Neuquén. Relatorio XVIII Congreso Geológico Argentino 4:37–47

Cohen K, Finney S, Gibbard P, Fan J-X (2013) The ICS International Chronostratigraphic Chart. Episodes 36:199–204

Collins W (2002) Nature of extensional accretionary orogens. Tectonics 21(4) 1024:1–12

COPLA (2017) The Argentine Continental Margin: between 35° and 55° South latitude in the context of article 76 of the United Nations Convention on the Law of the Sea. Ministerio de Relaciones Exteriores y Culto, Comisión Nacional del Límite Exterior de la Plataforma Continental, www.plataformaargentina.gob.ar

Cortés J (1987) Descripción Geológica de la Hoja 42 h, Puerto Lobos, Provincia del Chubut, Carta Geológico-Económica de la República Argentina, Escala 1:200.000. Dir Nac Min Geol Boletín 202:1–95

Dalla Salda L, Cingolani C, Varela R (1992) Early Paleozoic orogenic belt of the Andes in southwestern South America: result of Laurentia-Gondwana collision? Geology 20:617–620

Dalla Salda L, Cingolani C, Varela R (1993) A pre-Carboniferous tectonic model in the evolution of southern South America. Comptes Rendus XII ICC-P:371–384

Ewing M, Ludwig W, Ewing J (1963) Geophysical investigations in the submerged Argentine coastal plain. Part I, Buenos Aires to Peninsula Valdés. Geol Soc Am Bull 74(3):275–292

Ferrill D, Dunne W (1989) Cover deformation above a blind duplex: an example from West Virginia, USA. J Struct Geol 11:421–431

Forsythe R (1982) The Late Paleozoic to Early Mesozoic evolution of Southern South America: a plate tectonic interpretation. J Geol Soc London 139:671–682

Franke D, Neben S, Ladage S et al (2007) Margin segmentation and volcano-tectonic architecture along the volcanic margin off Argentina/Uruguay, South Atlantic. Mar Geol 244:46–67

Fryklund B, Marshall A, Stevens J (1996) Cuenca del Colorado. In: Ramos V, Turic M (eds) Geología y Recursos Naturales de la Plataforma Continental Argentina, Relatorio XIII Cong Geol Arg y III Cong Exp Hidroc, vol 8, pp 135–158

Geiser P (1988) Mechanisms of thrust propagation: some examples and implications for the analysis of overthrust terranes. J Struct Geol 10:829–845

Giacosa R (1999) El basamento pre-Silúrico del extremo este del Macizo Nordpatagónico y del Macizo del Deseado. In: Caminos R (ed) Geología Argentina. IGRM-SEGEMAR Anales 29(5):118–123

Giacosa R (2001) Zonas de cizalla frágil-ductil neopaleozoicas en el nordeste de la Patagonia. Rev Asoc Geol Arg 56(2):131–140

Giacosa R (2020) Basement control, sedimentary basin inception and early evolution of the Mesozoic basins in the Patagonian foreland. J S Am Ear Sci 97:102407

Giacosa R, Paredes J (2001) Estructura de las metamorfitas del Paleozoico temprano en el Arroyo Salado. Macizo Norpatagónico, Río Negro. Rev Asoc Geol Arg 56(2):141–149

Giacosa R, González P, Silva Nieto D, et al (2014) Complejo Igneometamórfico Cáceres: una nueva unidad metamórfica de alto grado en el basamento de Gastre, Macizo Nordpatagónico (Chubut). Proc XIX Cong Geol Arg (CD):S21–19

González P et al (2020) Geochemistry and geochronology of the Early Paleozoic arc magmatism in Northern Patagonia terrane. J So Am Earth Sci **(submitted and in review)**

González P, Cucchi R (1994) Las metamorfitas y granitoides de Mencué, Macizo Norpatagónico, Río Negro, Argentina. Proc VII Cong Geol Chile 2:1051–1056

González P, Poiré D, Varela R (2002) Hallazgo de trazas fósiles en la Formación El Jagüelito y su relación con la edad de las metasedimentitas, Macizo Norpatagónico Oriental, Río Negro. Rev Asoc Geol Arg 57:35–44

González P, Varela R, Sato A et al (2008a) Metamorfismo regional Ordovícico y estructura de la Ectinita El Jagüelito al SO de Sierra Grande, Río Negro. Proc XVII Cong Geol Arg 2:849–850

González P, Varela R, Sato A et al (2008b) Dos fajas estructurales distintas en el Complejo Mina Gonzalito (Río Negro). Proc XVII Cong Geol Arg 2:847–848

González P, Sato A, Llambías E, Varela R (2008c) Geología del Corrimiento Piedras Coloradas, basamento ígneo-metamórfico de Las Grutas, Río Negro. Proc XVII Cong Geol Arg 2:845–846

González P, Varela R, Sato A et al (2010) Evidencias geológicas y paleontológicas en la Formación El Jagüelito para la conexión Patagonia-Antártida durante el Paleozoico inferior. Proc X Cong Arg Paleont y Bioest y VII Cong Latinoam Paleont, Resumen 24:48

González P, Tortello M, Damborenea S (2011a) Early Cambrian archeocyathan limestone blocks in low-grade meta-conglomerate from El Jagüelito Formation (Sierra Grande, Río Negro, Argentina). Geologica Acta 9(2):159–173

González P, Greco G, Varela R, et al (2011b) Patrón metamórfico invertido en la Formación El Jagüelito de la Herradura del Salado, basamento Norpatagónico, Río Negro. Proc XVIII Cong Geol Arg (CD):85–86

Gonzalez P, Sato A, Naipauer M et al (2018) Patagonia-Antarctica Early Paleozoic conjugate margins: Cambrian synsedimentary silicic magmatism, U-Pb dating of K-bentonites, and related volcanogenic rocks. Gond Res 63:186–225

Gozalvez M (2009) Petrografía y edad $^{40}Ar/^{39}Ar$ de leucogranitos peraluminosos al oeste de Valcheta: Macizo Nordpatagónico (Río Negro). Rev Asoc Geol Arg 64:285–294

Greco G, González S, Sato A et al (2014) Nueva datación en circones detríticos para el Complejo Mina Gonzalito, Provincia de Río Negro. Proc XIX Cong Geol Arg (CD) 1:1454–1455

Greco G, González P, González S et al (2015) Geology, structure and age of the Nahuel Niyeu Formation in the Aguada Cecilio area, North Patagonian Massif, Argentina. J S Am Earth Sci 62:12–32

Greco G, González S, Sato A et al (2017) The Nahuel Niyeu basin: a Cambrian forearc basin in the eastern North Patagonian Massif. J So Am Earth Sci 79:111–136

Gregori D, Kostadinoff J, Strazzere L (2008) Tectonic significance and consequences of the Gondwanide orogeny in northern Patagonia, Argentina. Gond Res 14:429–450

Gregori D, Kostadinoff J, Alvarez G et al (2013) Preandean geological configuration of the eastern North Patagonian Massif. Argentina Geos Front 4(6):693–708

Guidotti C, Sassi F (1986) Classification and correlation of metamorphic facies series by means of muscovite bo data from low-grade metapelites. Neues Jahrb Mineral Abh 153:363–380

Haller M (1981) Descripción Geológica de la Hoja 43h "Puerto Madryn", Provincia del Chubut. Serv Geol Nac Boletín 184:1–41

Hashimoto M (1966) On the prehnite–pumpellyite metagreywacke facies. J Geol Soc Japan 72:253–255

Hervé F, Calderón M, Fanning M et al (2018) The country rocks of Devonian magmatism in the North Patagonian Massif and Chaitenia. Andean Geol 45(3):301–317

Ince E, Barthelmes F, Reißland S et al (2019) ICGEM-15 years of successful collection and distribution of global gravitational models, associated services and future plans. Earth Syst Sci Data 11:647–674

Jamtveit B, Austrheim H (2010) Metamorphism: the role of fluids. Elements 6:153–158

Kaasschieter J (1965) Geología de la Cuenca del Colorado. Acta Geológica Lilloana 7:251–269

Kostadinoff J (1992) Configuración y litología del basamento geofísico en el litoral comprendido entre Viedma y San Antonio Oeste, Provincia de Río Negro. Rev Asoc Geol Arg 47(3):317–321

Kostadinoff J, Gregori D, Raniolo A (2005) Configuración geofísica-geológica del sector norte de la provincia de Río Negro. Rev Asoc Geol Arg 60(2):368–376

Kretz R (1983) Symbols for rock-forming minerals. Am Mineral 68:277–279

Kübler B, Pittion J, Héroux Y et al (1979) Sur le pouvoir réflecteur de la vitrinite dans quelques roches du Jura, de la molasse et des Nappes préalpines, helvétiques et penniques (Suisse occidentale et Haute-Savoie). Eclogae Geol Helv 72(2):347–373

Lardeaux J (2014) Deciphering orogeny: a metamorphic perspective. Examples from European Alpine and Variscan belts. Part I: alpine metamorphism in the western Alps-a review. Bull Soc Géol France 185:93–114

Liégeois J (1998) Preface - Some words on the post-collisional magmatism. Lithos 45:xv-xvii

Llambías E, Varela R, Basei M, Sato A (2002) Deformación y metamorfismo Neopaleozoico en Yaminué, Macizo Norpatagónico (40°50'S, 67°40'W): su relación con la Fase Orogénica San Rafael y el arco de los Gondwánides. Proc XV Cong Geol Arg 3:123–128

Martínez Dopico C, López de Luchi M, Rapalini A et al (2017) U-Pb SHRIMP dating of detrital zircon grains of the Colo Niyeu Formation: extending the latest Neoproterozoic to Cambrian peri-Gondwana realm into the central North Patagonian Massif. Proc XX Cong Geol Arg S-15:66–72

McKenzie D, Morgan W (1969) The evolution of triple junctions. Nature 224:125–133

Merriman R, Frei M (1999) Patterns of very low-grade metamorphism in pelitic rocks. In: Frey M, Robinson D (eds) Low-grade metamorphism. Blackwell Sciences Ltd, Oxford, pp 61–107

Merriman R, Peacor D (1999) Very low-grade metapelites; mineralogy, microfabrics, and measuring reaction progress. In: Frey M,

Robinson D (eds) Low-grade metamorphism. Blackwell Sciences Ltd, Oxford, pp 10–60
Miyashiro A (1967) Orogeny, regional metamorphism, and magmatism in the Japanese Islands. Medd Dansk Geol Foren 17:390–446
Miyashiro A (1973) Paired and unpaired metamorphic belts. Tectonophysics 17(3):241–254
Miyashiro A (1994) Metamorphic Petrology. Taylor & Francis Group, reprinted, London and New York, pp416
Naipauer M, González P, Varela R et al (2011) Edades U-Pb (LA-ICP-MS) en circones detríticos del Miembro Polke, Formación Sierra Grande, Río Negro: ¿Una nueva unidad Cambro-Ordovícica? Proc XVIII Cong Geol Arg (CD) 1:113–114
Núñez E, Cucchi R (1990) Estratigrafía del sector noroccidental del Macizo Nordpatagónico en los alrededores de Mencué, provincia del Río Negro, República Argentina. Proc XI Cong Geol Arg 2:125–128
Oriolo S, Oyhantçabal P, Wemmer K, Siegesmund S (2017) Contemporaneous assembly of Western Gondwana and final Rodinia break-up: implications for the supercontinent cycle. Geos Front 8(6):1431–1445
Page Chamberlain C (1986) Evidence for the repeated folding of isotherms during regional metamorphism. J Petrol 27(1):63–89
Pankhurst R, Rapela C, Fanning C (2000) Age and origin of coeval TTG, I- and S-type granites in the Famatinian belt of NW Argentina. Transac Royal Soc Edinburgh Earth Sci 91:151–168
Pankhurst R, Rapela C, Fanning C et al (2006) Gondwanide continental collision and the origin of Patagonia. Earth-Sci Rev 76:235–257
Pankhurst R, Rapela C, López de Luchi M et al (2014) The Gondwana connections of northern Patagonia. J Geol Soc 171:313–328
Paterson S, Vernon R, Fowler T Jr (1991) Aureole tectonics. In: Kerrick D (ed) Contact Metamorphism. Mineral Soc Am Rev Mineral 26:673–722
Ramos V (1975) Geología del sector oriental del Macizo Nordpatagónico entre Aguada Capitán y la Mina Gonzalito, provincia de Río Negro. Rev Asoc Geol Arg 30:274–285
Ramos V (1984) Patagonia: ¿un continente Paleozoico a la deriva? Proc IX Congreso Geológico Argentino 2:311–325
Ramos V (1988) Late Proterozoic-early Paleozoic of South America—a collisional history. Episodes 11:168–174
Ramos V (2004) Cuyania, an exotic block to Gondwana: review of historical success and the present problems. Gond Res 7(4):1009–1026
Ramos V (2008) Patagonia: a Paleozoic continent adrift? J S Am Earth Sci 26:235–251
Ramos V, Naipauer M (2014) Patagonia: where does it come from? J Iberian Geol 40(2):367–379
Ramos V, Vujovich G (1993) Laurentia-Gondwana connection: a South American perspective. GSA Abst with Prog A:232
Ramos V, Jordan T, Allmendinger R et al (1986) Paleozoic Terranes of the Central Argentine Chilean Andes. Tectonics 5:855–880
Ramos V, Riccardi A, Rolleri E (2004) Límites naturales del norte de la Patagonia. Rev Asoc Geol Arg 59:785–786
Ramos V, Vujovich G, Martino R, Otamendi J (2010) Pampia: a large cratonic block missing in the Rodinia supercontinent. J Geodyn 50:243–255
Ramos V, Mosquera A, Folguera A et al (2011) Evolución tectónica de los Andes y del Engolfamiento Neuquino adyacente. In: Leanza H, et al. (eds) Geología y Recursos Naturales de la provincia del Neuquén. Asociación Geológica Argentina, Argentina, pp 335–348
Ramos V (2018) The Famatinian Orogen along the Protomargin of Western Gondwana: evidence for a nearly continuous Ordovician magmatic arc between Venezuela and Argentina. In: Folguera A, et al. (eds) The evolution of the Chilean-Argentinean Andes, Springer Earth System Sciences. Springer, Cham
Rapalini A, López de Luchi M, Martínez Dopico C et al (2010) Did Patagonia collide with Gondwana in the Late Paleozoic? Some insights from a multidisciplinary study of magmatic units of the North Patagonian Massif. Geológica Acta 8(4):349–371
Rapalini A, López de Luchi M, Tohver E et al (2013) The South American ancestry of the North Patagonian Massif: geochronological evidence for an autochthonous origin? Terra Nova 25:337–342
Rapalini A, Geuna S, Franceschinis P et al (2018) Paleogeographic and kinematic constraints in the tectonic evolution of the pre-Andean basement blocks. In: Folguera A, et al. (eds) The evolution of the Chilean-Argentinean Andes, Springer Earth System Sciences. Springer, Cham
Rapela C, Pankhurst R, Casquet C et al (1998) The pampean orogeny of the southern proto-Andes: Cambrian continental collision in the Sierras de Córdoba. In: Pankhurst R, Rapela C (eds) The proto-andean margin of Gondwana. Geol Soc Lond Spec Pub 142:181–217
Rapela C, Verdecchia S, Casquet C et al (2016) Identifying Laurentian and SW Gondwana sources in the Neoproterozoic to Early Paleozoic metasedimentary rocks of the Sierras Pampeanas: Paleogeographic and tectonic implications. Gond Res 32:193–212
Renda E, Álvarez D, Prezzi C, et al. (2019) Inherited basement structures and their influence in foreland evolution: a case study in Central Patagonia, Argentina. Tectonophy 772:article 228232
Robinson D (1987) The transition from diagenesis to metamorphism in extensional and collision settings. Geology 15:866–869
Robinson D, Bevins R (1986) Incipient metamorphism in the Lower Palaeozoic marginal basin of Wales. J Metamorph Geol 4:101–113
Rustan J, Cingolani C, Cicardi A, et al (2013) Lower Silurian trilobites from the Northern Patagonia Sierra Grande Formation. Ameghiniana 50 (6) Suplemento 2013, Resumen R 68
Sato A, González P, Llambías E (2003) Evolución del orógeno Famatiniano en la Sierra de San Luis: magmatismo de arco, deformación y metamorfismo de bajo a alto grado. Rev Asoc Geol Arg 58(4):487–504
Sato A, Basei M, Tickyj H et al (2004) Granodiorita El Sótano: plutón jurásico deformado aflorante en el basamento de Las Grutas, Macizo Norpatagónico Atlántico. Rev Asoc Geol Arg 59(4):591–600
Schmitt R, Fragoso R, Collins A (2018) Suturing Gondwana in the Cambrian: the Orogenic Events of the Final Amalgamation. In: Siegesmund S, Basei M, Oyhantçabal P, Oriolo S (eds) Geology of Southwest Gondwana, Regional Geology Reviews. Springer, Cham
Schulmann K, Schaltegger U, Jezek J et al (2002) Rapid burial and exhumation during orogeny: Thickening and synconvergent exhumation of thermally weakened and thinned crust (Variscan orogen in Western Europe). Am J Sci 302:856–879
Siccardi A, Uriz N, Rustán J, et al (2014) Hirnantian?-Early Silurian brachiopods from the Sierra Grande Formation (North Patagonian Massif, Río Negro Province, Argentina). 4th International Palaeontological Congress, Abstract Volume:807
Siegesmund S, Steenken A, Martino R et al (2009) Time constraints on the tectonic evolution of the Eastern Sierras Pampeanas (Central Argentina). Intern J Earth Sci 99:1199–1226
Starr P, Pattison D, Ames D (2019) Mineral assemblages and phase equilibria of metabasites from the prehnite-pumpellyite to amphibolite facies, with the Flin Flon Greenstone Belt (Manitoba) as a type example. J Metamor Geol 38(1):71–102
Stipp M, Stunitz H, Heilbronner R, et al (2002) Dynamic recrystallization of quartz: correlation between natural and experimental conditions. In: De Meer S et al (eds), Deformation Mechanisms, Rheology and Tectonics: current status and future perspectives. Geol Soc, Spe Public, London, pp 171–190

Tickyj H, Llambías E, Melchor R (2002) Ordovician rocks from La Pampa province, Argentina. In: Aceñolaza F (ed), Aspects on the Ordovician system of Argentina, Serie Correlación Geológica 16:257–266

Turner J, Baldis B (1978) La estructura transcontinental del límite septentrional de la Patagonia. Proc VII Con Geol Arg 2:225–238

Uriz N, Cingolani C, Chemale F Jr et al (2011) Isotopic studies on detrital zircons of Silurian-Devonian siliciclastic sequences from Argentinean North Patagonia and Sierra de la Ventana regions: comparative provenance. Intern J Earth Sci 100:571–589

Uriz N, Cingolani C, Taboada A (2019) Edades U-Pb en circones detríticos de las secuencias metasedimentarias pre-carboníferas de la zona de Esquel, Chubut. Proc XVI Reu Arg Sedim T-S 5:65

Varela R, Basei M, Sato A et al (1998) Edades isotópicas Rb/Sr y U/Pb en rocas de Mina Gonzalito y Arroyo Salado. Macizo Norpatagónico Atlántico, Río Negro, Argentina. Proc X Cong Latinoam Geología y VI Cong Nac Geol Econom 1:71–76

Varela R, Basei M, González P et al (2008) Granitoides Famatinianos y Gondwánicos en Sierra Grande. Nuevas edades radimétricas método U-Pb. Proc XVII Cong Geol Arg 2:914–915

Varela R, Basei M, González P et al (2011a) Accretion of Grenvillian terranes to the southwestern border of the Rio de la Plata craton, western Argentina. Intern J Ear Sci 100:243–272

Varela R, González P, Basei M et al (2011b) Edad del Complejo Mina Gonzalito: Revisión y nuevos datos. Proc XVIII Con Geol Arg Abstracts (CD) 1:127–128

Varela R, González P, Philipp R et al (2014) Isótopos de estroncio en calcáreos del noreste patagónico: resultados preliminares. Rev Asoc Geol Arg 71:526–536

von Gosen W (2002) Polyphase structural evolution in the northeastern segment of the North Patagonian Massif (southern Argentina). J S Am Earth Sci 15:591–623

von Gosen W (2003) Thrust tectonics in the North Patagonian Massif (Argentina): implications for a Patagonia Plate. Tectonics 22(1):1005

von Gosen W, Prozzi C (2010) Pampean deformation in the Sierra Norte de Córdoba, Argentina: implications for the collisional history at the western pre-Andean Gondwana margin. Tectonics 29:TC2012

Wakabayashi J (2004) Tectonic mechanisms associated with P-T paths of regional metamorphism: alternatives to single-cycle thrusting and heating. Tectonoph 392:193–218

Walther J, Orville P (1982) Volatile production and transport in regional metamorphism. Contrib Mineral Petrol 79(3):252–257

Warr L, Cox S (2016) Correlating illite (Kübler) and chlorite (Árkai) "crystallinity" indices with metamorphic mineral zones of the South Island, New Zealand. Appl Clay Sci 134:164–174

Warr L, Ferreiro Mählmann R (2015) Recommendations for Kübler Index standardization. Clay Miner 50:282–285

Willner A, Sepúlveda F, Hervé F (2009) Conditions and timing of pumpellyite-actinolite-facies metamorphism in the Early Mesozoic frontal accretionary prism of the Madre de Dios Archipelago (Latitude 50°20′S; Southern Chile). J Petrol 50(11):2127–2155

Willner A, Tassinari C, Rodrigues J et al (2014) Contrasting Ordovician high- and low-pressure metamorphism related to a microcontinent-arc collision in the Eastern Cordillera of Perú (Tarma province). J S Am Earth Sci 54:71–81

Yamamoto H (1993) Contrasting metamorphic P-T-time paths of the Kohistan granulites and tectonics of the western Himalayas. J Geol Soc 150:843–856

Affiliations

Pablo D. González[1] · Maximiliano Naipauer[2] · Ana M. Sato[3] · Ricardo Varela[3] · Miguel A. S. Basei[4] · María Cecilia Cábana[5] · Silvio R. F. Vlach[4] · Martín Arce[6] · Martín Parada[6]

Maximiliano Naipauer
maxinaipauer@gl.fcen.uba.ar

Ana M. Sato
sato@cig.museo.unlp.edu.ar

Ricardo Varela
ricardovarela4747@gmail.com

Miguel A. S. Basei
baseimas@usp.br

María Cecilia Cábana
mccabana@unrn.edu.ar

Silvio R. F. Vlach
srfvlach@usp.br

Martín Arce
marce@unrn.edu.ar

Martín Parada
mnparada@unrn.edu.ar

[1] Instituto de Investigación en Paleobiología y Geología (UNRN-CONICET), Av. Julio A. Roca 1242, R 8332 EXZ, General Roca (Río Negro), Argentina

[2] Instituto de Estudios Andinos "Don Pablo Groeber" (UBA-CONICET), Güiraldes 2160, Ciudad Universitaria, Pabellón II, C 1428 EHA, Ciudad Autónoma de Buenos Aires, Argentina

[3] Centro de Investigaciones Geológicas (UNLP-CONICET), Diagonal 113 No 275, B 1904 DPK, La Plata (Buenos Aires), Argentina

[4] Centro de Pesquisas Geocronológicas (CPGeo), Instituto de Geociências, Conselho Nacional de Desenvolvimento Científico e Tecnológico (CNPq), Universidade de São Paulo, Cidade Universitária, Rua Do Lago 562, São Paulo CEP 05508-080, Brazil

[5] Universidad Nacional de Río Negro, Instituto de Investigación en Paleobiología y Geología, Geomatics Laboratory, Av. Julio A. Roca 1242. R 8332 EXZ, General Roca (Río Negro), Argentina

[6] Universidad Nacional de Río Negro, Instituto de Investigación en Paleobiología y Geología, XRD and Electron Microscopy Laboratory, Av. Julio A. Roca 1242. R 8332 EXZ, General Roca (Río Negro), Argentina